nature metabolism

Article

https://doi.org/10.1038/s42255-023-00921-9

Efferocytosis-induced lactate enables the proliferation of pro-resolving macrophages to mediate tissue repair

Received: 15 May 2023

Accepted: 5 October 2023

Published online: 27 November 2023

Check for updates

David Ngai [1], Maaike Schilperoort [1] & Ira Tabas [1,2]

The clearance of apoptotic cells by macrophages (efferocytosis) prevents necrosis and inflammation and activates pro-resolving pathways, including continual efferocytosis. A key resolution process in vivo is efferocytosis-induced macrophage proliferation (EIMP), in which apoptotic cell-derived nucleotides trigger Myc-mediated proliferation of pro-resolving macrophages. Here we show that EIMP requires a second input that is integrated with cellular metabolism, notably efferocytosis-induced lactate production. Lactate signalling via GPR132 promotes Myc protein stabilization and subsequent macrophage proliferation. This mechanism is validated in vivo using a mouse model of dexamethasone-induced thymocyte apoptosis, which elevates apoptotic cell burden and requires efferocytosis to prevent inflammation and necrosis. Thus, EIMP, a key process in tissue resolution, requires inputs from two independent processes: a signalling pathway induced by apoptotic cell-derived nucleotides and a cellular metabolism pathway involving lactate production. These findings illustrate how seemingly distinct pathways in efferocytosing macrophages are integrated to carry out a key process in tissue resolution.

The clearance of apoptotic cells (ACs), known as efferocytosis, is a critical process mediated mostly by macrophages to promote tissue repair and homeostasis[1–4]. Efferocytosis prevents pro-inflammatory secondary necrosis and promotes the secretion of pro-resolving factors, such as TGF-β and IL-10, to suppress inflammation and promote tissue resolution[1–4]. Pro-resolving factors can, in turn, promote efferocytosis, particularly the sequential uptake of multiple ACs by a single macrophage known as continual efferocytosis[5]. This process forms a physiologically important efferocytosis-resolution positive-feedback cycle[1–4].

Macrophage functions, including those involved in efferocytosis and resolution, is profoundly affected by intracellular metabolism and metabolic by-products. For example, lactate produced by glycolytic metabolism plays an active role in pro-resolution signalling in immune cells, including macrophages[6–9]. Two recent studies have shown that efferocytosis can drive increased glycolysis to produce lactate, which stimulates macrophage secretion of pro-resolving factors and promotes continual efferocytosis[8,9]. Another form of macrophage metabolism that occurs during efferocytosis is 'cargo' metabolism, whereby metabolites released during phagolysosomal degradation of ACs, such as nucleic acids[10–12], can trigger pro-resolving pathways and continual efferocytosis in efferocytosing macrophages. A physiologically important example of this principle is a macrophage proliferation pathway activated by AC-derived nucleotides, which functions in vivo to promote AC clearance and tissue resolution by expanding the pool of pro-resolving macrophages[10]. This process, termed efferocytosis-induced macrophage proliferation (EIMP), involves two convergent pathways: (1) an ERK1/2 pathway activated

[1]Department of Medicine, Columbia University Irving Medical Center, New York, NY, USA. [2]Departments of Physiology and Cell Biology, Columbia University Irving Medical Center, New York, NY, USA. e-mail: dhn2111@columbia.edu; iat1@columbia.edu

when ACs engage the macrophage MerTK receptor; and (2) a DNA-PK–mTORC2–Akt pathway activated by AC-derived oligonucleotides after the engulfed ACs are degraded in phagolysosomes. These pathways result in increased transcription of *Myc* messenger RNA (mRNA), leading to Myc-mediated cell cycling[10]. As Myc protein stability is an important determinant of Myc protein levels[13–19], we wondered how this aspect of Myc regulation factored into EIMP.

Glycolytic metabolism and lactate have been shown to promote proliferation in other cell types, such as vascular smooth muscle cells and regulatory T cells[20,21]. Moreover, lactate has been linked to the activation of the NAD^+-dependent protein deacetylase, SIRT1, which is a protein deacetylase known to deacetylate Myc and promote its stability[14–16]. We therefore proposed that efferocytosis-induced lactate (EIL) could promote EIMP through the stabilization of Myc protein by SIRT1-mediated deacetylation. In support of this idea, we show that lactate production during efferocytosis is necessary to increase Myc protein through protein stabilization and is required for EIMP. Myc stabilization requires SIRT1, which is downstream of a PKA–AMPK–NAD^+ pathway, and PKA is activated by secreted lactate acting through the G-protein-coupled receptor 132 (GPR132). Inhibition or genetic targeting of the rate-limiting enzyme for lactate production, lactate dehydrogenase A (LDHA), reduces Myc protein and EIMP both in vitro and in vivo, leading to impaired macrophage proliferation and AC clearance and increased tissue necrosis. Thus, distinct metabolic pathways in efferocytosing macrophages, one involving AC cargo and the other involving lactate production, are integrated to enable the expansion of pro-resolving macrophages and subsequent tissue repair.

Results

EIL increases Myc and is necessary for EIMP

To test the role of EIL in EIMP, we inhibited LDHA with FX11 (ref. 22) in efferocytosing murine bone marrow-derived macrophages (BMDMs) and human monocyte-derived macrophages (HMDMs). We first confirmed that efferocytosis increases lactate production and that lactate levels are lowered by treatment with the LDHA inhibitor FX11 (Extended Data Fig. 1a). As previously reported[10], incubating macrophages with ACs to trigger efferocytosis results in an increase in cell number after 24 hours, and we found that this increase was blocked by FX11 and restored by adding back lactic acid to the FX11-inhibited macrophages (Fig. 1a,b). In the context of our hypothesis that EIL might stabilize Myc protein to promote EIMP (below), we assessed whether EIL promotes AC-induced Myc protein expression. We used three methods of blocking LDHA activity: siLdha-treated BMDMs, which led to roughly 65% silencing of *Ldha* (Extended Data Fig. 1b); FX11-treated BMDMs and BMDMs from $Ldha^{fl/fl}$;$LysMCre^{+/-}$ (M-LDHA-KO (knockout)) mice. All three strategies resulted in an attenuation of AC-induced Myc protein expression (Fig. 1c–e). FX11 did not affect primary AC engulfment (Extended Data Fig. 1c), indicating that the decrease in Myc in LDHA-deficient or LDHA-inhibited macrophages was not merely due to decreased AC uptake. Furthermore, loss of AC-induced Myc protein expression in LDHA-KO or FX11-treated macrophages could be rescued by exogenous addition of lactic acid in a dose-dependent manner (Fig. 1f and Extended Data Fig. 1d). The rescue was not due to the acidity of lactic acid since the addition of sodium lactate could also rescue AC-induced Myc protein in LDHA-inhibited macrophages (Extended Data Fig. 1e). The link between lactate and EIMP was through Myc, as the decrease in EIMP that occurs with Myc silencing could not be rescued by exogenous lactic acid (Fig. 1g and Extended Data Fig. 1f). Moreover, lactic acid treatment in the absence of ACs had no effect on basal Myc protein expression or cell number (Extended Data Fig. 1g,h), consistent with the importance of first increasing *Myc* mRNA through the efferocytosis-induced p-ERK and AC-nucleotide/DNase2a/DNA-PK pathways[10]. Exogenous lactic acid attenuates AC-induced Myc in efferocytosing macrophages with normal EIL production (Extended Data Fig. 1i), suggesting that excessive lactic acid somehow partially suppresses the efferocytosis–Myc pathway. Indeed, while 10 mM lactic acid rescues AC-induced Myc protein expression in FX11-treated macrophages, 25 mM lactic acid does not (Extended Data Fig. 1j). Together, these data show that EIL drives Myc production and EIMP, but there is an upper limit to the concentration of lactic acid that can promote this process.

EIL stabilizes Myc protein through Myc deacetylation

We propose that EIL increases Myc protein in a step that follows and requires *Myc* mRNA induction by the AC-nucleotide–DNase2a–DNA-PK pathway[10]. If so, then lactic acid should not be able to rescue EIMP if this initial *Myc* mRNA-inducing pathway is blocked. One way to block the AC-nucleotide–DNA-PK pathway is to silence DNase2a, as DNase2a-mediated hydrolysis of AC-DNA to oligonucleotides in phagolysosomes is required to activate DNA-PK and induce *Myc*[10]. Accordingly, we evaluated the effect of lactic acid on Myc in small-interfering Dnase2a (siDnase2a)-treated efferocytosing macrophages. As expected[10], siDnase2a treatment of efferocytosing macrophages blunted AC-induced Myc protein expression, and Myc protein expression was not rescued by lactic acid in the siDnase2a-treated macrophages (Fig. 2a). This latter finding is consistent with the idea that lactate stabilizes Myc protein following DNase2a-dependent induction of *Myc* mRNA in efferocytosing macrophages. Further, if lactate promotes EIMP by promoting Myc protein stabilization and not *Myc* transcription, then blocking EIL should not lower AC-induced *Myc* mRNA. Indeed, in both BMDMs and HMDMs, the AC-induced increase in *Myc* mRNA was not blocked by FX11 (Fig. 2b,c). In a similar vein, while lactate secreted from efferocytosing macrophages could act on neighbouring non-efferocytosing macrophages, these macrophages should not respond with increased Myc protein, as non-efferocytosing macrophages lack the initial AC-induced increase in *Myc* mRNA. Consistent with this prediction, Myc protein expression was increased in AC^+ but not AC^- macrophages, and it was reduced by siLdha only in AC^+ macrophages (Fig. 2d).

Given that acetylation of Myc promotes its proteasomal degradation[14,15,17], we determined whether the loss of AC-induced Myc protein expression resulting from LDHA-KO could be rescued by the proteasome inhibitor MG132. In control ($Ldha^{fl/fl}$) BMDMs, MG132 treatment boosted AC-induced Myc protein expression, suggesting that there is a basal level of Myc degradation in efferocytosing macrophages (Fig. 2e, $Cre^{-/-}$ data). Most importantly, whereas AC-induced Myc protein expression was reduced by LDHA-KO in vehicle-treated BMDMs, it was not reduced by LDHA-KO in MG132-treated BMDMs (Fig. 2e, $Cre^{+/-}$ data). These data suggest that EIL promotes AC-induced Myc protein expression by reducing the proteasomal degradation of Myc protein. MG132 treatment of non-efferocytosing macrophages had no significant effect on Myc protein expression compared with untreated efferocytosing macrophages (Extended Data Fig. 1k), which is consistent with the above data that lactic acid alone has no effect on Myc protein expression or macrophage proliferation. This finding further supports the notion of a two-hit process consisting of AC-cargo-mediated *Myc* mRNA transcription[10] followed by EIL-mediated Myc protein stabilization.

Given that acetylation at lysine-323 (Ac-K323) of Myc enhances Myc proteasomal degradation[16], we wanted to test the hypothesis that EIL promotes Myc deacetylation. However, assaying acetyl-Myc is challenging, as total Myc is markedly upregulated by ACs, and proteasomal degradation causes the loss of acetyl-Myc[14,15,17]. We therefore assessed the effect of LDHA inhibition ± lactic acid in macrophages incubated with ACs and MG132, that is, to keep total Myc relatively comparable among groups and to prevent the proteasomal loss of acetyl-Myc. Using this strategy, we were able to show that LDHA inhibition with FX11 increased both the acetyl-Myc to total Myc ratio and the acetyl-Myc to β-actin ratio and that lactic acid treatment of these LDHA-inhibited

https://doi.org/10.1038/s42255-023-00921-9

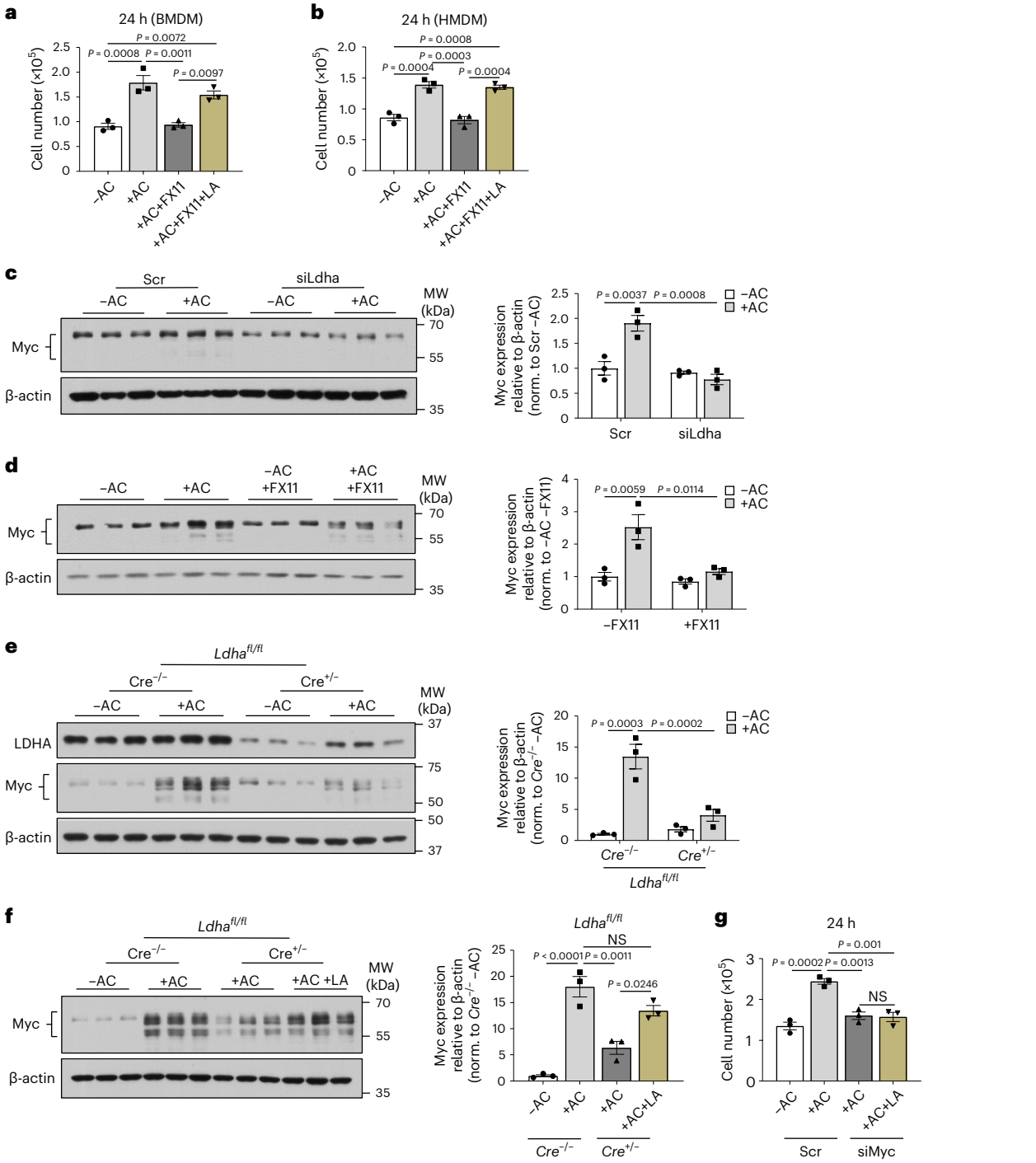

Fig. 1 | LDHA-dependent lactate production during efferocytosis increases Myc protein and promotes EIMP. a,**b**, BMDMs (**a**) or HMDMs (**b**) were incubated with or without ACs for 45 min, chased for 24 h ± 50 µM FX11 and ± 10 mM lactic acid (LA), and quantified for cell number ($n = 3$). **c**, BMDMs transfected with 50 nM scrambled or Ldha siRNA for 72 h were incubated with or without ACs for 45 min, chased for 3 h and immunoblotted for Myc ($n = 3$). MW, molecular weight. norm., normalized. **d**, BMDMs were incubated with or without ACs for 45 min, chased for 3 h ± 50 µM FX11 and immunoblotted for Myc ($n = 3$). **e**, *Ldha*$^{fl/fl}$ or *Ldha*$^{fl/fl}$;*LysMCre*$^{+/-}$ BMDMs were incubated with or without ACs for 45 min, chased for 3 h and immunoblotted for Myc ($n = 3$). **f**, *Ldha*$^{fl/fl}$ or *Ldha*$^{fl/fl}$;*LysMCre*$^{+/-}$ BMDMs were incubated with or without ACs for 45 min, chased for 3 h ± 10 mM lactic acid and immunoblotted for Myc ($n = 3$). **g**, BMDMs transfected with 50 nM scrambled or Myc siRNA were incubated with or without ACs for 45 min, chased for 24 h ± 10 mM lactic acid and quantified for cell number ($n = 3$). Bars represent means ± s.e.m. Statistics were performed by one-way ANOVA in **a** and **b** and **f** and **g** or two-way ANOVA in **c**–**e**. NS, not significant ($P > 0.05$).

macrophages lowered both ratios to the levels seen without LDHA inhibition (Fig. 2f). These combined data support the idea that after *Myc* transcription is induced by the AC-cargo pathway[10], EIL deacetylates and stabilizes Myc protein in efferocytosing macrophages to enable macrophage proliferation.

EIL-induced SIRT1 activation increases Myc protein and EIMP

Sirtuin-1 (SIRT1) is an NAD^+-dependent protein deacetylase that has been shown previously in other cell types to deacetylate and stabilize Myc protein[14–16,18], and SIRT1 has also been implicated in efferocytosis and inflammation resolution[12,23]. Moreover, lactic acid generated by

https://doi.org/10.1038/s42255-023-00921-9

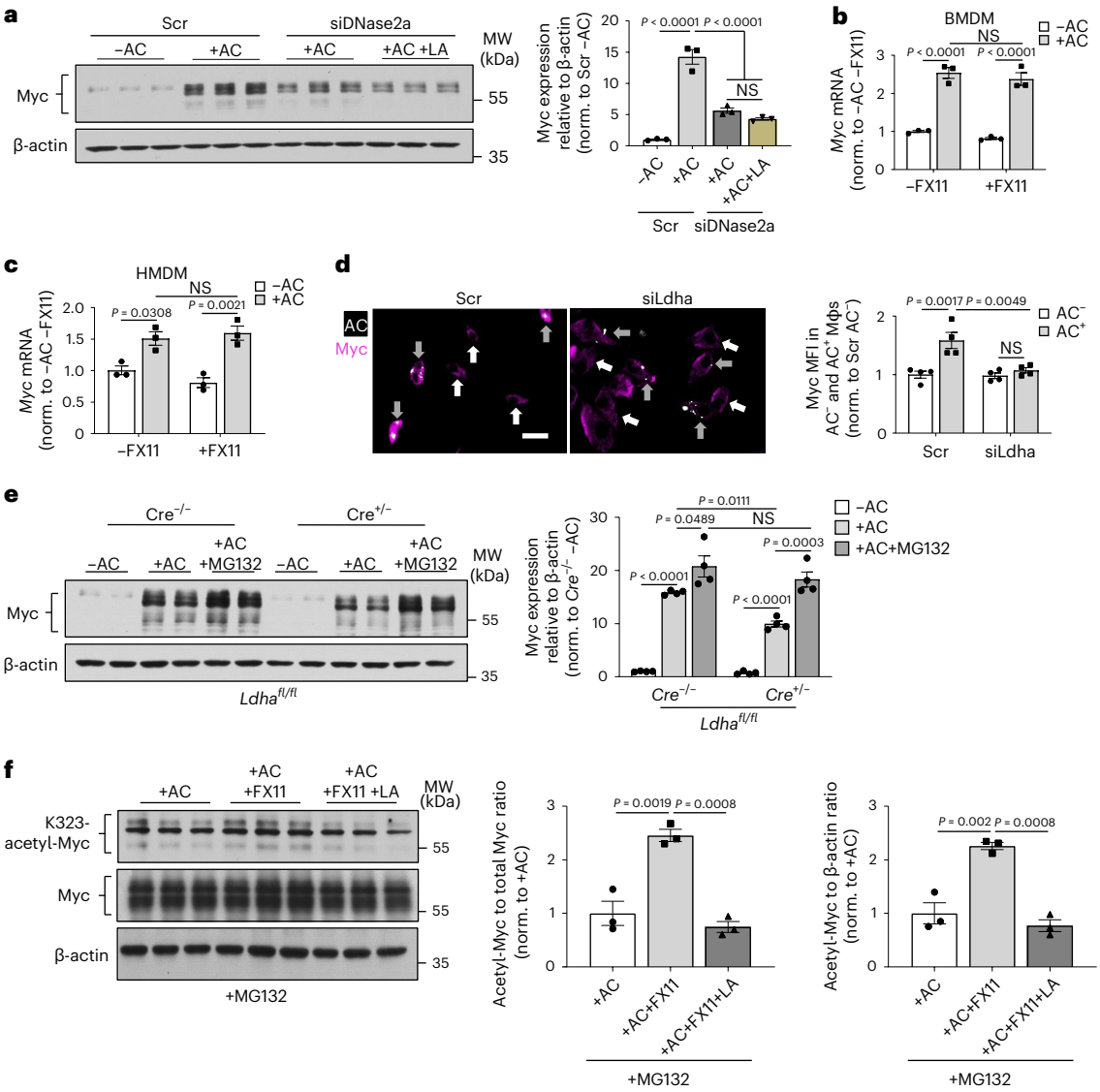

Fig. 2 | EIL stabilizes AC-induced Myc protein through decreased Myc acetylation, which occurs following AC-nucleotide/DNase2a-mediated *Myc* transcription. a, BMDMs transfected with 50 nM scrambled or Dnase2a siRNA for 72 h were incubated with or without ACs for 45 min, chased for 3 h and immunoblotted for Myc ($n = 3$). **b**,**c**, BMDMs (**b**) or HMDMs (**c**) were incubated with or without ACs for 45 min, chased for 3 h ± 50 µM FX11 and assayed for *Myc* mRNA ($n = 3$). **d**, BMDMs transfected with 50 nM scrambled or Ldha siRNA for 72 h were incubated with PKH26-labelled ACs for 45 min, chased for 3 h, fixed with 4% PFA and immunostained for Myc. Cells were imaged with a 20x objective. Scale bar, 20 µm ($n = 4$). **e**, *Ldha*$^{fl/fl}$ or *Ldha*$^{fl/fl}$;*LysMCre*$^{+/-}$ BMDMs were incubated with or without ACs for 45 min, chased for 3 h ± 10 µM MG132 and immunoblotted for Myc ($n = 4$). **f**, BMDMs were incubated with ACs for 45 min, chased for 3 h ± 50 µM FX11 and ± 10 mM lactic acid in the presence of 10 µM MG132 and immunoblotted for K^{323}-acetyl-Myc, total Myc and β-actin ($n = 3$). Bars represent means ± s.e.m. Statistics were performed by one-way ANOVA in **a** and **f** or two-way ANOVA in **b**–**e**. NS, $P > 0.05$.

exercise has been reported to activate SIRT1 in the brain[24]. We therefore considered the hypothesis that EIL uses SIRT1 to stabilize Myc protein and enable EIMP. In support of this idea, we found that efferocytosis activates SIRT1, which was attenuated by FX11 treatment and restored with exogenous lactic acid (Fig. 3a). Efferocytosis also increased SIRT1 protein expression, and partial silencing of SIRT1 lowered AC-induced Myc protein expression (Fig. 3b). SIRT1-silencing caused a modest decrease in primary efferocytosis (Extended Data Fig. 2a), which was probably too small to explain the large decrease in AC-induced Myc protein expression. Nonetheless, we tested the effect of the SIRT1 inhibitor EX527 (ref. 25) added after AC uptake and found that this treatment also lowered AC-induced Myc protein expression (Fig. 3c). Moreover, exogenous lactic acid could not rescue the reduction in AC-induced Myc protein expression following EX527 treatment (Extended Data Fig. 2b), which is consistent with SIRT1 acting downstream of lactate. In addition, EX527 did not affect AC-induced *Myc* mRNA expression, indicating that SIRT1 regulates Myc protein expression posttranscriptionally (Fig. 3d). Most importantly, SIRT1 inhibition blocked EIMP in both mouse BMDMs and HMDMs as measured by total cell number (Fig. 3e,f). Finally, to directly link SIRT1 to stabilization of Myc against proteasomal degradation (above), we showed that the reduction in AC-induced Myc protein expression by EX527 was abrogated by MG132 (Fig. 3g) and that EX527 treatment of efferocytosing macrophages increased acetyl-Myc levels (Fig. 3h). These combined data support the idea that EIL-induced SIRT1 activation deacetylates and stabilizes Myc protein, thereby enabling EIMP.

CSF1-induced macrophage proliferation, which is a common form of proliferation observed in inflammation, does not involve the

https://doi.org/10.1038/s42255-023-00921-9

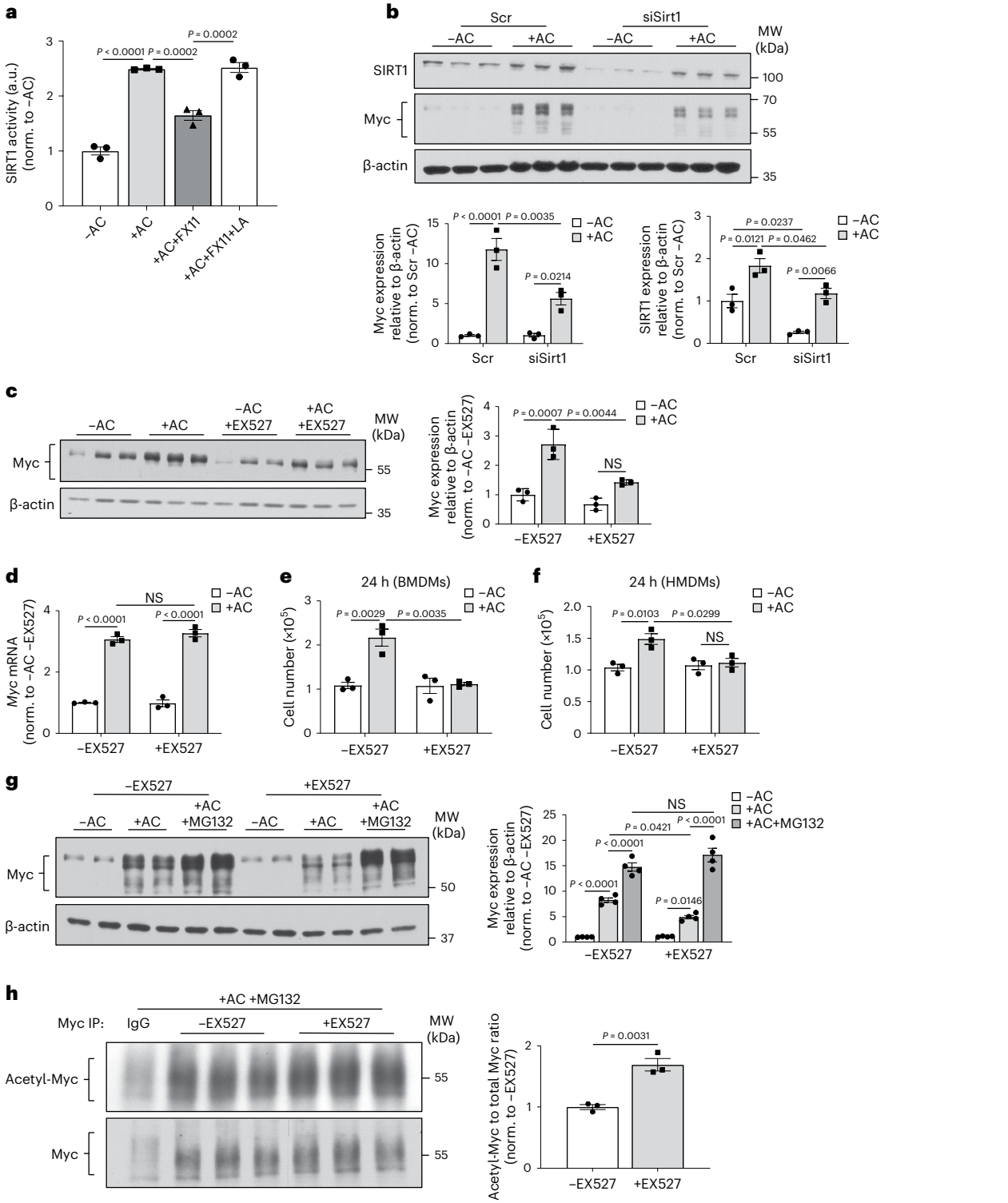

Fig. 3 | EIL activates SIRT1, which stabilizes Myc by deacetylation and promotes EIMP. a, BMDMs were incubated with or without ACs for 45 min, chased for 1 h ± 50 μM FX11 and ± 10 mM LA, and assayed for SIRT1 activity ($n = 3$). **b**, BMDMs transfected with 50 nM scrambled or Sirt1 siRNA for 72 h were incubated with or without ACs for 45 min, chased for 3 h and immunoblotted for SIRT1 and Myc ($n = 3$). **c**, BMDMs were incubated with or without ACs for 45 min, chased for 3 h ± 10 μM EX527 and immunoblotted for Myc ($n = 3$). **d**, BMDMs were incubated with or without ACs for 45 min, chased for 3 h ± 10 μM EX527 and assayed for *Myc* mRNA ($n = 3$). **e**,**f**, BMDMs (**e**) or HMDMs (**f**) were incubated with or without ACs for 45 min, chased for 24 h ± 10 μM EX527 and quantified for cell number ($n = 3$). **g**, BMDMs were incubated with or without ACs for 45 min, chased for 3 h ± 10 μM EX527 and ± 10 μM MG132, and immunoblotted for Myc ($n = 4$). **h**, BMDMs were incubated with ACs for 45 min and then chased for 3 h ± 10 μM EX527, and cell extracts were immunoprecipitated (IP) with control IgG or anti-cMyc antibody. The immunoprecipitated protein was immunoblotted for acetylated lysine (acetyl-Myc) and total Myc ($n = 3$). Acetyl-Myc was quantified relative to total Myc. Bars represent means ± s.e.m. Statistics were performed by two-tailed Student's *t*-test in **h**, one-way ANOVA in **a** and two-way ANOVA in **b**–**g**. NS, $P > 0.05$.

AC-cargo-induced signalling pathway that occurs in EIMP[10]. Nonetheless, as CSF1 is known to both increase lactate production[26] and induce Myc expression[27] in macrophages, we investigated the LDHA–SIRT1 pathway in CSF1-treated macrophages. Both FX11 and EX527 attenuated CSF1-induced Myc protein expression (Extended Data Fig. 2c,d), which may suggest a common LDHA–SIRT1–Myc pathway in both CSF1-treated macrophages and efferocytosing macrophages. However, neither inhibitor blocked the increase in cell number in CSF1-treated macrophages beyond a minor trend (Extended Data Fig. 2e). These data are consistent with previous findings that inputs in addition to Myc are required to mediate proliferation in CSF1-treated macrophages[28]. Indeed, while silencing Myc markedly decreased proliferation in efferocytosing macrophages, there was only a minor, non-statistically significant trend in CSF1-treated macrophages (Extended Data Fig. 2f). We have also shown previously that silencing Bhlhe40, a key mediator of EIMP downstream of Myc, could abolish EIMP whereas it had no significant effect on CSF1 mediated proliferation[10]. These data further distinguish EIMP from CSF1-induced macrophage proliferation.

EIL stabilizes Myc through an AMPK–NAD^+–SIRT1 pathway

Several previous studies on lactate and SIRT1, although not related to Myc or proliferation, suggested to us a hypothesis as to how lactate might be linked to the SIRT1–Myc–EIMP pathway. SIRT1 is an NAD^+-dependent protein deacetylase[29]. In non-immune tissues such as skeletal muscle, AMPK (5′ AMP-activated protein kinase) has been shown to raise NAD^+ levels through the nicotinamide phosphoribosyl-transferase salvage pathway, which then activates SIRT1 (refs. 29,30). Other studies have reported that lactic acid can activate AMPK, for example, in skeletal muscle in vivo and BMDMs in vitro[7,31] and that efferocytosis can activate AMPK[32]. Given these previous observations, we proposed that EIL might activate AMPK, which would then increase the NAD^+ to NADH ratio and activate the SIRT1-mediated Myc-EIMP pathway. Consistent with this hypothesis, we found that both lactic acid treatment and incubation of macrophages with ACs raised the level of pAMPK, which indicates AMPK activation, and the lactic acid-induced increase in pAMPK in efferocytosing macrophages was prevented by LDHA silencing (Fig. 4a,b). Moreover, inhibition of AMPK with the inhibitor Compound C reduced AC-induced SIRT1 activity (Fig. 4c). Compound C also reduced AC-induced increases in both Myc protein (Fig. 4d) and EIMP, as measured by cell count (Fig. 4e). These effects were not caused by a decrease in AC uptake, as AMPK inhibition by Compound C did not affect primary efferocytosis (Extended Data Fig. 2g). Furthermore, AMPK inhibition did not blunt CSF1-dependent macrophage proliferation, indicating specificity for EIMP (Fig. 4f).

As mentioned, EIL might be linked to SIRT1 activation through an increase in the NAD^+ to NADH ratio[29]. Consistent with this idea, the addition of ACs to macrophages increased the NAD^+ to NADH ratio, and this increase was prevented by LDHA-KO and rescued by exogenous lactic acid treatment (Fig. 4g). To assess causation, FX11-treated macrophages were supplemented with or without the NAD^+ precursor, nicotinamide mononucleotide (NMN), to rescue NAD^+ levels and then assayed for Myc protein expression and proliferation. We found that the decreases in both Myc protein expression and cell number in FX11-treated AC-exposed macrophages were rescued by NMN (Fig. 4h,i). In addition, Compound C blunted the AC-induced increase in the NAD^+ to NADH ratio (Fig. 4j), and NMN supplementation of Compound C-treated cells, which restored the NAD^+ to NADH ratio (Extended Data Fig. 2h), rescued the decreases in both AC-induced Myc protein expression and cell number (Fig. 4k,l). In the absence of efferocytosis, NMN did not affect Myc protein expression (Extended Data Fig. 2i). Furthermore, NMN in these experiments was acting through SIRT1, as the loss of AC-induced Myc protein in SIRT1-silenced BMDMs could not be rescued by NMN (Extended Data Fig. 2j). Thus, EIL activates an AMPK–NAD^+–SIRT1 pathway to increase Myc protein expression and promote EIMP.

EIL activates AMPK through GPR132-PKA signalling

To determine how EIL activates AMPK, we considered the canonical mechanism of AMPK activation, namely, as a response to ATP depletion[33]. However, ATP levels do not change or slightly increase rather than decrease during and after AC uptake[8,12]. We therefore became interested in a cell-surface G-protein-coupled lactate receptor called GPR132, which was shown previously to be involved in lactate-mediated activation of a PKA–AMPK pathway in inflammatory macrophages[7]. If this pathway were relevant in our setting, EIL-induced Myc protein would require the release of lactate to the extracellular space to activate the cell-surface receptor. Indeed, partial silencing of the lactate transporter SLC16a1, which partially decreased the export of lactate from efferocytosing macrophages as previously reported[8,9] (Extended Data Fig. 3a,b), partially lowered Myc protein expression (Fig. 5a). We next explored the effect of the GPR132 inhibitor telmisartan[34] and the GPR132 activator ONC212 (ref. 35) on EIL-induced Myc protein expression. Telmisartan treatment resulted in a reduction of AC-induced Myc protein expression (Fig. 5b) and, conversely, the loss of AC-induced Myc protein expression in FX11-treated macrophages was rescued by ONC212 (Fig. 5c). As a complement to the telmisartan data, we showed that small-interfering RNA (siRNA) silencing of GPR132 lowered both AC-induced Myc protein expression and EIMP, as measured by cell number (Fig. 5d,e and Extended Data Fig. 3c). Moreover, siGpr132 blocked the ability of lactic acid to rescue Myc protein expression in FX11-treated macrophages (Extended Data Fig. 3d). *Gpr132* mRNA was increased in an LDHA-dependent manner when macrophages were incubated with ACs, suggesting a possible positive-feedback cycle driven by EIL (Extended Data Fig. 3e).

To probe the role of the GPR132 signalling molecule PKA, we first incubated macrophages with exogenous lactic acid and showed that this treatment increased phosphorylation of CREB (cAMP-response element binding protein) (Fig. 5f), which is a target of PKA and a marker for PKA activity. Further, incubation of macrophages with ACs increased pCREB (phosphorylated CREB), and this increase was reduced by LDHA-KO and restored by exogenous lactic acid (Fig. 5g). In addition, silencing GPR132 in AC-exposed macrophages lowered pCREB and pAMPK (Fig. 5h). Finally, treatment of AC-exposed macrophages with the PKA inhibitor H89 reduced pAMPK activation, Myc protein expression and EIMP, as measured by cell count (Fig. 5i–k).

In conclusion, while our previous study elucidated an AC-cargo pathway in efferocytosing macrophages that increases *Myc* mRNA[10], our new data suggest that EIMP requires a second, posttranscriptional process, namely, stabilization of Myc protein. This process is triggered by extracellular lactate resulting from efferocytosis-induced macrophage glycolysis and lactate export by SLC16a1 (refs. 8,9). Extracellular lactate activates a GPR132–PKA–AMPK pathway that increases the NAD^+ to NADH ratio, leading to SIRT1-mediated Myc protein deacetylation and stabilization. The increase in Myc protein from the combined actions of the AC-cargo pathway and EIL enable EIMP (Fig. 5l).

In vivo evidence that EIL promotes EIMP and tissue resolution

To evaluate the role of EIL in EIMP and efferocytosis in vivo, we used a model of acute apoptosis in which efferocytosis is required to promote tissue resolution. In this model, dexamethasone treatment of mice induces thymocyte apoptosis, followed by clearance of the apoptotic thymocytes by recruited thymic macrophages and then tissue resolution[10,11,36–38]. We conducted this experiment in irradiated mice transplanted with either control $Ldha^{fl/fl}$ bone marrow cells or $Ldha^{fl/fl}$ bone marrow cells transfected ex vivo with cell-permeable TAT-Cre before infusion to knockdown *Ldha* (LDHA-KD). In the LDHA-KD cohort, LDHA protein was decreased by roughly 50% in both bone marrow cells (Fig. 6a) and thymic macrophages (Fig. 6b), but not in non-macrophage $Mac2^-$ thymic cells (Fig. 6b). Moreover, the concentrations of immune cells in the circulation were similar in the LDHA-KD and control group mice, suggesting that haematopoietic LDHA-KD did not affect the

https://doi.org/10.1038/s42255-023-00921-9

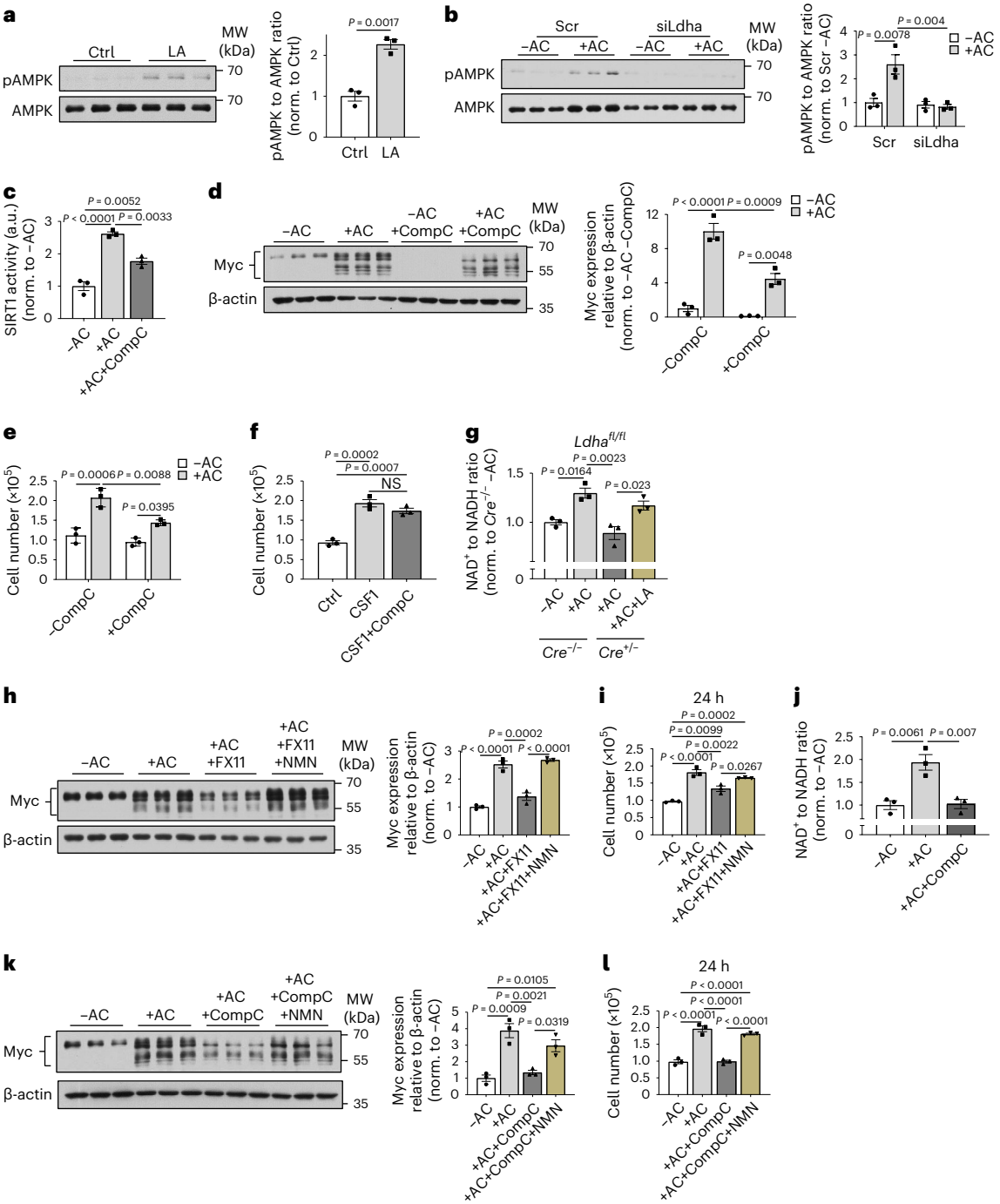

Fig. 4 | EIL activates AMPK, thereby increasing the NAD$^+$ to NADH ratio, SIRT1 activity, Myc protein and EIMP. a, BMDMs were incubated with or without ACs for 45 min, treated ± 10 mM lactic acid for 1 h and immunoblotted for pAMPK and total AMPK ($n = 3$). **b**, BMDMs transfected with 50 nM scrambled or Ldha siRNA for 72 h were incubated with or without ACs, chased for 1 h and immunoblotted for pAMPK and total AMPK ($n = 3$). **c**, BMDMs were incubated with or without ACs, chased for 1 h ± 10 μM CompC and assayed for SIRT1 activity ($n = 3$). **d**, BMDMs were incubated with or without ACs, chased for 3 h ± 10 μM Compound C (CompC) and immunoblotted for Myc ($n = 3$). **e**, BMDMs were incubated with or without ACs, chased for 24 h ± 10 μM CompC and quantified for cell number ($n = 3$). **f**, WT BMDMs were treated for 24 h with 50 ng ml^{-1} CSF1 ± 10 μM CompC and quantified for cell number ($n = 3$). **g**, *Ldha*$^{fl/fl}$ or *Ldha*$^{fl/fl}$; *LysMCre*$^{+/-}$ BMDMs were incubated with or without ACs, chased for 1 h ± 10 mM LA and assayed for the NAD$^+$ to NADH ratio ($n = 3$). **h**,**i**, BMDMs were incubated with or without ACs, chased for 3 h ± 50 μM FX11 and ± 500 μM NMN and immunoblotted for Myc ($n = 3$) (**h**) or chased for 24 h ± 50 μM FX11 and ± 500 μM NMN and quantified for cell number ($n = 3$) (**i**). **j**, BMDMs were incubated with or without ACs, chased for 1 h ± 10 μM CompC and assayed for the NAD$^+$ to NADH ratio ($n = 3$). **k**,**l**, BMDMs were incubated with or without ACs, chased for 3 h ± 10 μM CompC and ± 500 μM NMN and immunoblotted for Myc ($n = 3$) (**k**) or chased for 24 h ± 10 μM CompC and ± 500 μM NMN and quantified for cell number ($n = 3$) (**l**). Bars represent means ± s.e.m. Statistics were performed by two-tailed Student's *t*-test in **a**, one-way ANOVA in **c** and **f**–**l**, or two-way ANOVA in **d** and **e**. NS, $P > 0.05$. Ctrl, control.

https://doi.org/10.1038/s42255-023-00921-9

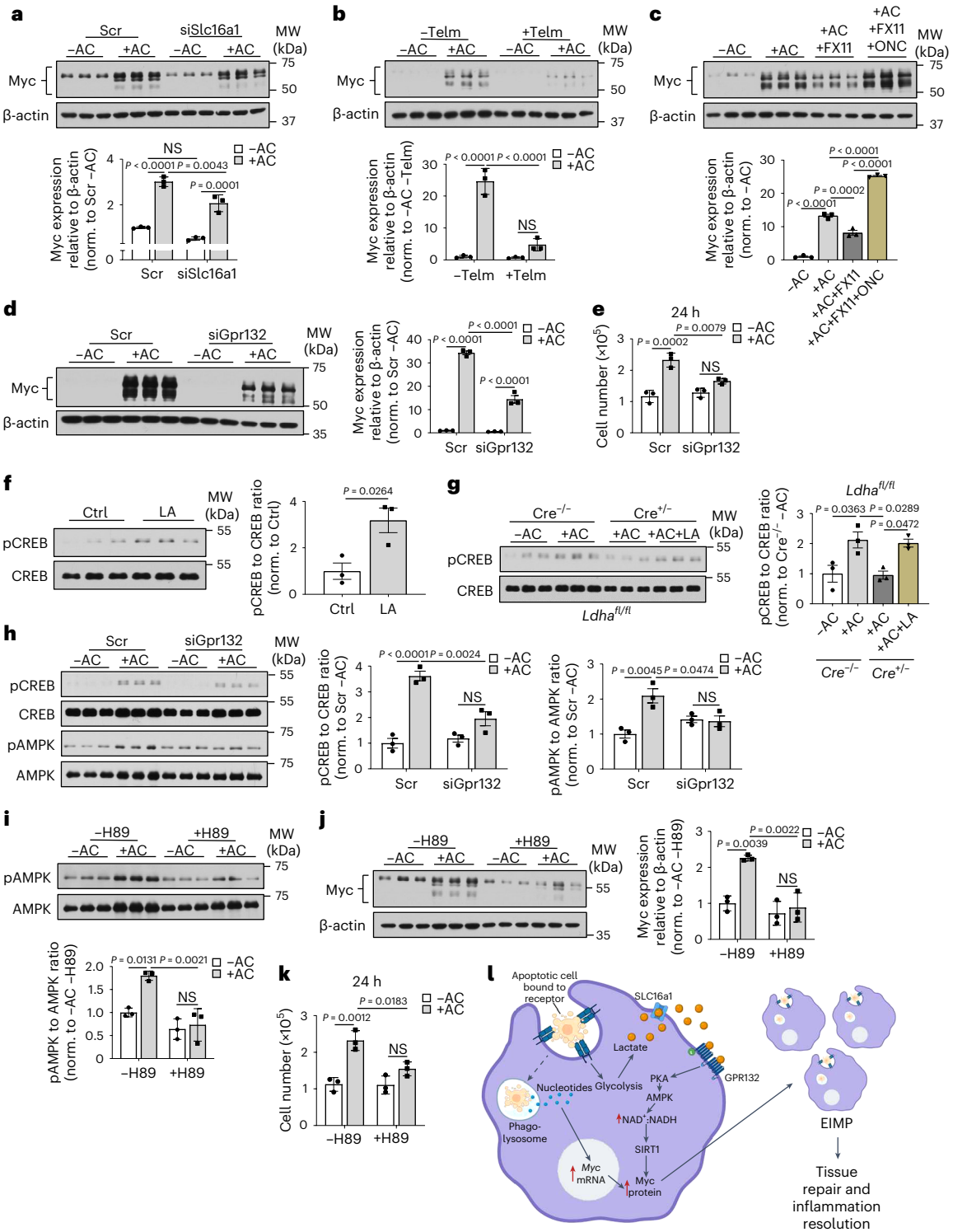

Fig. 5 | EIL activates AMPK by GPR132-PKA signalling, which increases Myc protein and EIMP. a, BMDMs transfected with 50 nM scrambled or Slc16a1 siRNA for 72 h were incubated with or without ACs for 45 min, chased for 3 h and immunoblotted for Myc ($n = 3$). **b**, BMDMs were incubated with or without ACs, chased for 3 h ± 10 μM telmisartan (Telm) and immunoblotted for Myc ($n = 3$). **c**, BMDMs were incubated with or without ACs, chased for 3 h ± 50 μM FX11 and ± 20 μM ONC212 (ONC) and immunoblotted for Myc ($n = 3$). **d**,**e**, BMDMs transfected with 50 nM scrambled (Scr) or Gpr132 siRNA for 72 h were incubated with or without ACs, chased for 3 h and immunoblotted for Myc ($n = 3$) (**d**) or chased for 24 h and quantified for cell number ($n = 3$) (**e**). **f**, BMDMs were treated ± 10 mM lactic acid for 1 h and then immunoblotted for pCREB and total CREB ($n = 3$). **g**, *Ldha*$^{fl/fl}$ or *Ldha*$^{fl/fl}$;*LysMCre*$^{+/-}$ BMDMs were incubated with or without ACs, chased for 1 h ± 10 mM LA and immunoblotted for pCREB and total CREB ($n = 3$). **h**, BMDMs transfected with scrambled or Gpr132 siRNA were incubated with or without ACs, chased for 1 h and immunoblotted for pCREB, total CREB, pAMPK and total AMPK ($n = 3$). **i**–**k**, BMDMs were incubated with or without ACs, chased for 1 h ± 10 μM H89 and immunoblotted for pAMPK and total AMPK ($n = 3$) (**i**), chased for 3 h ± 10 μM H89 and immunoblotted for Myc ($n = 3$) (**j**), or chased for 24 h ± 10 μM H89 and quantified for cell number ($n = 3$) (**k**). Bars represent means ± s.e.m. Statistics were performed by two-tailed Student's *t*-test in **f**, one-way ANOVA in **c** and **g**, or two-way ANOVA in **a**, **b**, **d**, **e** and **h**–**k**. NS, $P > 0.05$. **l**, Graphical depiction of how lactate produced by efferocytosis-induced macrophage glycolysis (EIMG)[9] integrates with the previously elucidated AC-derived nucleotide pathway[10] to enhance Myc protein levels and EIMP. This image was created with BioRender.com.

https://doi.org/10.1038/s42255-023-00921-9

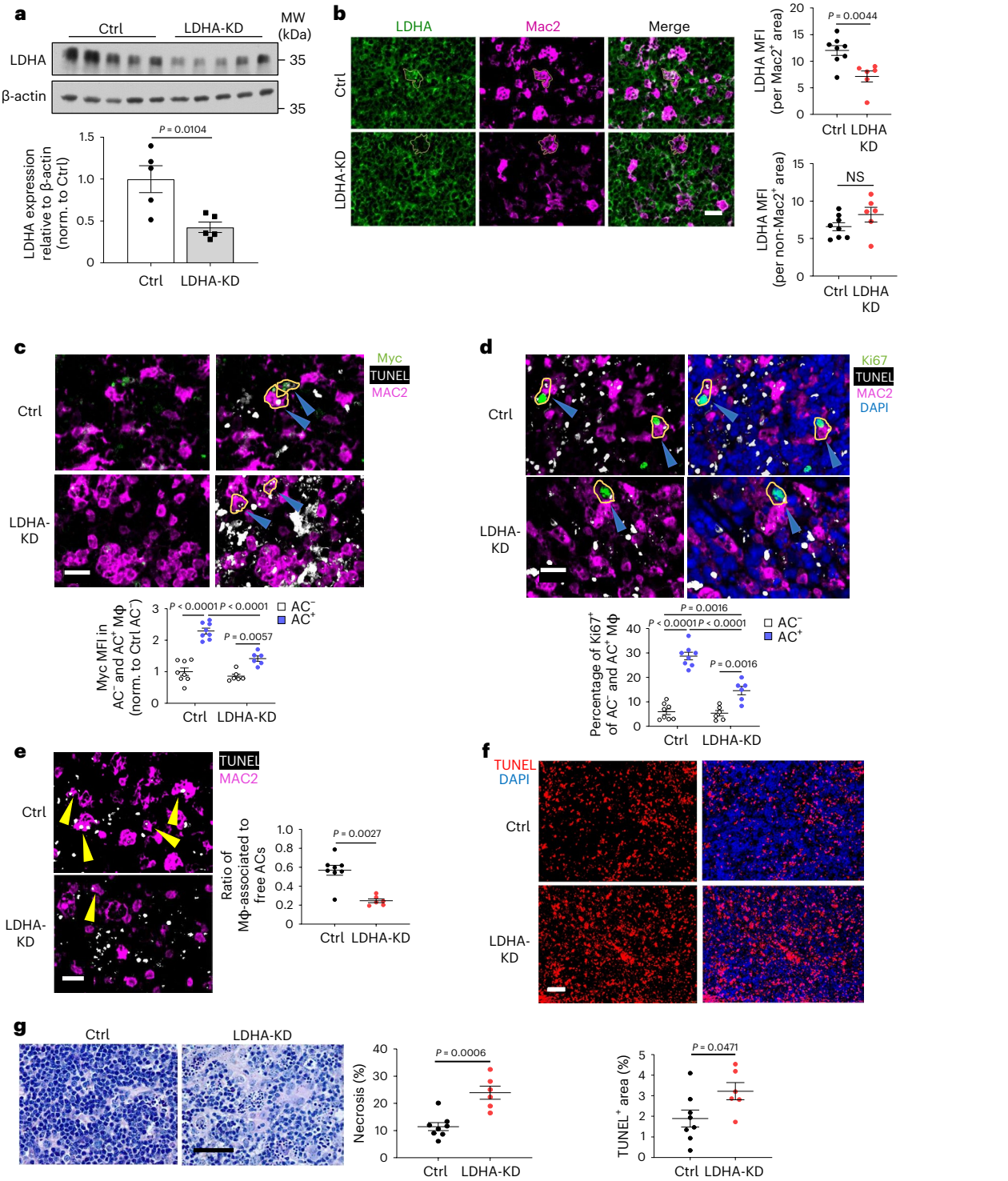

Fig. 6 | In vivo evidence that EIL promotes EIMP and tissue resolution. Bone marrow was isolated from male *Ldha*$^{fl/fl}$ mice, treated with 5 μM TAT-Cre to knockdown LDHA (LDHA-KD) or with vehicle (Ctrl) and transplanted into irradiated male C57BL/6J mice ($n = 8, 6$). After 4 weeks, the mice were subjected to a dexamethasone-thymus assay. **a**, Bone marrow cells isolated from mice were immunoblotted for LDHA ($n = 5$). **b**, Thymus sections were stained for LDHA (green) and Mac2 (magenta) and quantified for LDHA MFI in Mac2$^+$ and Mac2$^-$ areas ($n = 8, 6$). Scale bar, 20 μm. **c**, Thymus sections stained with TUNEL (white), anti-Myc (green) and anti-Mac2 (magenta) were quantified for Myc MFI in Mac2$^+$ TUNEL$^-$ (AC$^-$) and Mac2$^+$ TUNEL$^+$ (AC$^+$) cells ($n = 8, 6$). Scale bar, 20 μm. **d**, Thymus sections stained with TUNEL (white), anti-Ki67 (green) and anti-Mac2 (magenta) were quantified for the percentage Ki67$^+$ in Mac2$^+$ TUNEL$^-$ (AC$^-$) or Mac2$^+$ TUNEL$^+$ (AC$^+$) cells ($n = 8, 6$). Scale bar, 20 μm. **e**, Thymus sections were stained with TUNEL (white) and anti-Mac2 (magenta) and, as a measure of efferocytosis, the ratio of Mac2$^+$ macrophage-associated to free TUNEL$^+$ ACs was quantified ($n = 8, 6$). Scale bar, 20 μm. **f**, Thymus sections stained with TUNEL (red) were quantified for percentage TUNEL$^+$ area of total area ($n = 8, 6$). Scale bar, 50 μm. **g**, H&E-stained thymus sections were quantified for percentage necrotic area ($n = 8, 6$). Scale bar, 50 μm. Dot blots show means ± s.e.m. Statistics were performed by two-tailed Student's *t*-test in **a** and **b** and **f** and **g**, Mann–Whitney test in **e** and by two-way ANOVA in **c** and **d**. NS, $P > 0.05$.

systemic immune system (Extended Data Fig. 4a–f). Moreover, the circulating lactate concentration was also unchanged by knockdown of haematopoietic LDHA (Extended Data Fig. 4g). Next, we assayed Myc protein expression and EIMP in thymic macrophages by immunostaining for Myc protein and Ki67, a marker of proliferation, respectively. We looked at both macrophages carrying out efferocytosis, as marked by TUNEL$^+$ (terminal deoxynucleotidyl transferase dUTP nick end labelling) staining in the macrophage cytoplasm (AC$^+$ macrophages), as well as macrophages without cytoplasmic TUNEL staining (AC$^-$ macrophages). In control mice, there was a marked increase in both Myc and Ki67 in AC$^+$ thymic macrophages, but not AC$^-$ macrophages, as previously described[10] (Fig. 6c,d, Ctrl). However, both Myc protein expression and Ki67-positivity were substantially less in AC$^+$ macrophages in the thymi of LDHA-KD mice (Fig. 6c,d, LDHA-KD). There was no significant difference in Mac2$^+$ cell number in the two cohorts (Extended Data Fig. 4h). Continual efferocytosis is a critical process in the dexamethasone model due to the large number of apoptotic thymocytes[10,38,39]. In this context, we predicted that LDHA-KD, by preventing the pool of efferocytosis-capable macrophages from expanding, would show a defect in AC clearance. In line with this prediction, thymic macrophage efferocytosis, quantified as the ratio of macrophage-associated to free TUNEL$^+$ dead cells[10,11,36,37], was impaired in the LDHA-KD cohort (Fig. 6e). Further, consistent with impaired dead cell clearance, the thymi of LDHA-KD mice had more TUNEL$^+$ cells than control mouse thymi (Fig. 6f). Finally, a key functional endpoint of efferocytosis is prevention of tissue necrosis, and we found that thymic necrosis, quantified as the percentage area of hypocellular regions with fragmented nuclei, was increased in the LDHA-KD cohort (Fig. 6g). These combined data provide evidence that LDHA-dependent EIL is necessary for Myc expression and proliferation in efferocytosing macrophages in vivo and, most importantly, for the proper clearance of dead cells and tissue resolution.

Discussion

The findings herein illustrate how efferocytosing macrophages can integrate AC-cargo metabolism with macrophage glucose-lactate metabolism to carry out a key process in tissue resolution. In particular, the proliferation of efferocytosing macrophages (EIMP), which expands the pool of pro-resolving macrophages to mediate resolution, requires multiple inputs, consisting not only of MerTK-ERK1/2 and AC-nucleotide-DNA-PK-mTORC2-Akt signalling to increase *Myc* mRNA, as described previously[10], but also EIL to subsequently stabilize Myc protein.

Although the pathway described here is mediated by extracellular lactate, which could in theory act on all neighbouring macrophages, only AC$^+$ macrophages were found to have an LDHA-dependent increase in Myc expression. This finding is consistent with the idea that the EIL-Myc protein stabilization pathway is a process that follows increased *Myc* mRNA, which occurs only in efferocytosing macrophages. However, there may also be other paracrine pro-resolving effects of lactate that can affect both AC$^+$ and AC$^-$ macrophages, including other effects mediated by the GPR132–PKA–AMPK signalling pathway. For example, lactate can drive phenotypic switching of macrophages to a pro-resolving phenotype in certain contexts, including immunosuppression by cancer cells and the resolution of LPS-stimulated macrophage inflammation[6,7,40], and SLC16a1, as well as GPR132 and AMPK signalling, have been implicated in the reprogramming of macrophages to a pro-resolving phenotype[7,40–42]. A previous report showed that conditioned media from efferocytosing macrophages increased *Tgfb* and *Il10* mRNA in non-efferocytosing macrophages and that this did not occur using conditioned media from efferocytosing macrophages whose lactate transporters had been silenced[8]. However, a direct, mechanistic link between secreted lactate and pro-resolving mediators remains to be fully explored. Additionally, we showed recently that efferocytosis-induced glycolysis promotes continual efferocytosis in a lactate-dependent manner[9]. Although other cell types can contribute to the lactate pool, LDHA-KD in macrophages was sufficient to prevent EIMP in the dexamethasone-thymus experiment. EIMP macrophages have been shown to be very good at continual efferocytosis in vitro[10], and the capacity for continual efferocytosis in vitro has been tightly linked to apoptotic thymocyte clearance and tissue repair in this model[9,11,38,43]. However, there may exist other beneficial paracrine effects of EIL on tissue repair and the prevention of tissue necrosis. Paracrine effects are important, as only a subset of macrophages carry out efferocytosis[8–10,36], and thus EIL may be a mechanism by which the resolution-efferocytosis cycle may act more broadly.

Enhanced lactate secretion by efferocytosing macrophages could also have a beneficial role in tissue repair by signalling to other cell types[44,45]. For example, lactate has been shown to promote a synthetic phenotype in vascular smooth muscle cells and enhance their proliferation[20]. In atherosclerosis regression, a setting in which efferocytosis is reawakened after being relatively dormant in progressing lesions[11,46], a major hallmark is thickening of the fibrous cap mediated by synthetic vascular smooth muscle cell-derived cells, which contributes to plaque stabilization[47]. Accordingly, paracrine effects of EIL could have a role in enhancing this process. Lactate has also been shown to suppress the activation of effector CD4$^+$ and CD8$^+$ T cells[48], whereas lactate promotes the proliferation and activity of T-regulatory (T_{reg}) cells[21]. T_{reg} cells play a key role in polarizing macrophages to a pro-resolving, pro-efferocytic phenotype. for example, by enhancing the secretion of mediators such as IL-10 by macrophages to dampen inflammation and assist in tissue repair[46,49,50]. Thus, paracrine effects of EIL may play a role in promoting the efferocytosis-resolution cycle in settings in which T_{reg} cells play important roles, such as in atherosclerosis regression[46,50].

Our data show a direct role for lactate in EIMP via activation of the lactate receptor GPR132, leading to Myc stabilization and subsequent EIMP. However, the NAD$^+$ that is generated by this GPR132–AMPK pathway and/or by the upstream glycolysis–pyruvate–LDHA pathway[9,51] may further enhance efferocytosis-induced glycolysis[8,9], thereby forming a positive-feedback pathway. Future studies will be necessary to determine whether such a feedback pathway is operational in efferocytosing macrophages and, if so, whether it contributes to efferocytosis-induced resolution processes, including continual efferocytosis[9] and EIMP.

Both inflammatory macrophages and efferocytic macrophages can undergo proliferation and increase glycolysis to enhance lactate secretion[8–10,52]. However, macrophages do not undergo EIMP in inflammatory settings, and the kinetics and mechanisms of glycolysis are different between inflammatory macrophages and efferocytosing macrophages[9,10]. Inflammatory macrophages have a prolonged metabolic shift towards increased glycolysis, whereas efferocytosing macrophages have a transient burst in glycolysis[9]. We show here that if the lactate concentration is too high, AC-induced Myc expression is blunted, and thus the transient increase in glycolysis during efferocytosis may produce an optimal amount of lactate to sustain EIMP. Related to this point, in inflammatory diseases such as sepsis and atherosclerosis, increased circulating lactate is associated with disease severity[53,54], whereas efferocytosis occurs locally and is transient and thus would probably not be associated with higher levels of circulating lactate. Thus, it is possible that the elevated levels of lactate in inflammatory conditions may be detrimental or at least be a marker of pathophysiologic processes. Conversely, in conditions in which the inflammatory load is lower and efferocytosis is higher, such as in early atherosclerosis[55] and atherosclerosis regression[11], we suggest that lactate may be beneficial, which is supported by the dexamethasone-thymus data herein. Consistent with this idea, atherosclerosis is accelerated in GPR132-KO mice[56], which could be due in part from defects of the EIL–EIMP pathway in early atherosclerosis. In atherosclerosis regression, we have previously shown that blocking the AC-cargo–EIMP pathway through siDnase2a or siRictor nanoparticles prevents plaque stabilization[10]. Future studies are warranted

to determine whether blocking the EIL–EIMP pathway would yield a similar result.

GPR132 is known to be downregulated in LPS-induced inflammatory macrophages[7], which may be a contributing factor as to why inflammatory macrophages are unable to undergo EIMP despite being able to perform efferocytosis[10]. Lactate infusion in initially healthy mice was shown to increase GPR132 expression in adipose tissue macrophages[7], which is consistent with our data showing that efferocytosis induces *Gpr132* in an LDHA-dependent manner. This pathway may form a positive-feedback loop and contribute to the beneficial, pro-resolving effects of lactate infusion observed in humans. For example, ischaemic postconditioning through the infusion of lactated Ringer's solution (sodium lactate solution) resulted in an attenuation of ischaemia-reperfusion injury in myocardial infarction patients[57]. Exercise also transiently increases circulating lactic acid, which could be a contributing factor in the ability of exercise to protect against chronic inflammatory diseases[58]. From a therapeutic viewpoint, the findings here also raise the possibility that direct activation of GPR132 through pharmacologic agonists such as ONC212 could reawaken the dormant efferocytosis-resolution cycle that drives many chronic inflammatory diseases[2,35].

Methods

Cell lines

L-929 fibroblasts (CCL-1) and Jurkat T-lymphocytes (TIB-152) were obtained from ATCC. Both cell lines were cultured in DMEM supplemented with 10% heat-inactivated fetal bovine serum (HI-FBS) and 100 U ml^{-1} penicillin-streptomycin (Gibco). Cells were incubated at 37 °C with 5% CO_2.

Experimental animals

Animal protocols used were approved by Columbia University's Institutional Animal Care and Use Committee and were cared for according to National Institutes of Health (NIH) guidelines for the care and use of laboratory animals. The mice were socially housed in standard cages at 22 °C and with a 12-hour light-dark cycle in a barrier facility with ad libitum access to food and water. Male C57BL/6J mice (JAX, catalogue no. 000664), 8–10 weeks old, were used as bone marrow-transplantation (BMT) recipient mice for the dexamethasone-thymus experiment. Male *Ldha*$^{fl/fl}$ mice on the C57BL/6J background (JAX, catalogue no. 030112), 8–10 weeks old, were used as the bone marrow donors for this experiment. Mice of the same age and similar weight were randomly assigned to experimental and control groups.

BMT

Eight to ten-week-old C57BL/6J male mice (JAX) were irradiated with 10 Gγ with a caesium-137 γ-emitting irradiator (Gamma cell 40, MSD Nordion). Bone marrow cells collected from *Ldha*$^{fl/fl}$ mice (JAX, catalogue no. 030112) were incubated with 5 μM TAT-CRE Recombinase (Millipore) for 30 min to delete the *Ldha* gene. Bone marrow cells were then rinsed twice with PBS. *Ldha*$^{fl/fl}$ bone marrow cells not treated with TAT-Cre Recombinase were used as the control. Then 4 h after irradiation, 2.5×10^6 bone marrow cells were administered to recipient mice by tail vein injection. Recipient mice were allowed to recover for 4 weeks and given water containing 10 mg ml^{-1} neomycin for the first 3 weeks. These mice were then used for the dexamethasone-thymus assay.

Dexamethasone-thymus assay

Male mice transplanted with control or *Ldha*-deleted bone marrow were injected intraperitoneally with 250 μg dexamethasone (Sigma) in PBS. Eighteen hours after injection, the thymi were harvested, fixed in 10% formalin, embedded in paraffin and sectioned at a thickness of 5 μm. Sections were stained as described below under Immunofluorescence staining and microscopy. Efferocytosis was quantified as the ratio of Mac2$^+$-associated TUNEL$^+$ cells to free TUNEL$^+$ cells. Macrophage proliferation was assessed by quantifying % Ki67$^+$ in Mac2$^+$ TUNEL$^+$ or Mac2$^+$ TUNEL$^-$ cells. Myc expression was assessed by measuring Myc mean fluorescence intensity (MFI) in Mac2$^+$ TUNEL$^+$ or Mac2$^+$ TUNEL$^-$ cells. To measure necrotic area, H&E-stained thymic sections were imaged and regions with hypocellularity and fragmented nuclei were quantified. Male mice were used on the basis of evidence that female mice are more protected from dexamethasone-induced thymocyte apoptosis than male mice[59].

Mouse BMDMs

Bone marrow cells were isolated from the femurs of 8–10-week-old male C57BL/6J mice or from 6-week-old *Ldha*$^{fl/fl}$ mice or *Ldha*$^{fl/fl}$; *LysMCre*$^{+/-}$ mice and were cultured for 7 days in BMDM differentiation medium, which was DMEM supplemented with 10% (v/v) HI-FBS; 100 U ml^{-1} penicillin and 100 U ml^{-1} streptomycin (Corning) and 20% (v/v) L-929 cell-conditioned medium. Femurs from *Ldha*$^{fl/fl}$ mice and *Ldha*$^{fl/fl}$; *LysMCre*$^{+/-}$ mice were generously provided by L. Becker (University of Chicago). Cells were incubated at 37 °C in a 5% CO_2 incubator.

HMDMs

Peripheral blood mononuclear cells were isolated from the buffy coats of anonymous healthy adult donors with informed consent (New York Blood Center) using Histopaque-1077 (Sigma). Isolated cells were rinsed and cultured for 7–14 days in RPMI-1640 medium with L-glutamine (10-040; Corning) supplemented with 10% (v/v) HI-FBS (Gibco), 10 U ml^{-1} penicillin and 100 U ml^{-1} streptomycin (Corning) and 10 ng ml^{-1} GM-CSF (PeproTech). The University Institutional Review Board and Health Insurance Portability and Accountability Act guidelines were followed.

Generation of ACs and incubation with macrophages

Jurkat cells were resuspended in PBS and irradiated with a 254-nm ultraviolet lamp for 15 min to induce apoptosis. To fluorescently label ACs, irradiated ACs were pelleted by centrifugation, resuspended in Diluent C (Sigma), mixed with Diluent C containing PKH26 (red) (Sigma) and incubated at 37 °C for 5 min. The labelling reaction was halted with an equal volume of HI-FBS. ACs were pelleted by centrifugation, resuspended in PBS and incubated at 37 °C for 2–3 h. The ACs were collected by centrifugation, resuspended in fresh PBS, added to macrophages at a 5 to 1 number ratio of ACs to macrophages and incubated for 45 min at 37 °C. The volume ratio of the ACs in PBS to culture medium was 1/10. The macrophage monolayers were then rinsed with PBS to remove unbound ACs and chased for 1, 3 or 24 h in full medium with or without the addition of 50 μM FX11 (Sigma), 10 μM EX527 (Sigma), 10 μM Compound C (Sigma), 10 μM H89 (Sigma), 10 μM MG132 (Sigma), 10 mM lactic acid (Sigma), 500 μM NMN (Sigma), 10 μM telmisartan (MedChemExpress) or 20 μM ONC212 (MedChemExpress).

Lactate assay

Macrophages were seeded at 200,000 cells per well in 24-well plates in BMDM differentiation medium. The BMDMs, including those transfected with 50 nM scrambled siRNA or Slc16a1 siRNA for 72 h, were incubated with ACs, then chased for 1 or 3 h in 200 μl of low-serum DMEM (DMEM supplemented with 1% (v/v) HI-FBS) ± 50 μM FX11. Media was collected and assayed using a lactate assay kit from Sigma-Aldrich (catalogue no. MAK064) according to the manufacturer's instructions.

siRNA transfection

Macrophages were seeded at roughly 60% confluency in BMDM differentiation media. Scrambled siRNA or targeted siRNA (Dharmacon ON-TARGETplus SMARTpool siRNA) in Opti-MEM reduced-serum medium (Gibco) was transfected at a final concentration of 50 nM with Lipofectamine RNAiMAX (Life Technologies). After 18 h, the medium was changed to fresh BMDM differentiation medium and incubated for an additional 54 h before use.

Cell counting

Macrophages were seeded at 100,000 per well in a 12-well plate in 10% HI-FBS DMEM. Macrophages that were treated with ACs were chased for 24 h with or without various inhibitors. For experiments with M-CSF, macrophages were treated with 50 ng ml^{-1} M-CSF (Peprotech) with or without the inhibitors for 24 h. The BMDMs were detached with 10 mM EDTA in PBS on ice by gentle scraping, and HMDMs were detached with 0.25% trypsin-EDTA and repetitive, gentle pipetting. Collected cells were counted using a Countess II Automated Cell Counter (Invitrogen).

Immunoblotting

BMDMs were lysed in 2× Laemmli sample buffer (Bio-Rad) with 50 mM β-mercaptoethanol (Sigma) and lysates were boiled at 95–100 °C for 5 min. Lysates were loaded onto 4–20% SDS–PAGE gradient gels (Invitrogen) and run at 120 V for 90 min. Protein was transferred onto a 0.45-µm nitrocellulose membrane at 250 mA for 100 min. Membranes were blocked for 1 h with 5% skim milk in Tris-buffered saline with Tween-20 (TBST). Membranes were then incubated overnight at 4 °C with primary antibody diluted in 5% skim milk in TBST. Membranes were washed three times for 5 min with TBST before incubation with HRP-conjugated secondary antibodies at room temperature for 1–2 h and washed three times for 5 min with TBST. The following antibodies were used: rabbit anti-SIRT1 (CST 9475; 1:1,000), rabbit anti-LDHA (ProteinTech 19987-1-AP; 1:1,000), rabbit anti-pAMPK (CST 2535; 1:1,000), rabbit anti-AMPK (CST 5831; 1:1,000), rabbit anti-pCREB (CST 9198; 1:1,000), rabbit anti-CREB (CST 4820; 1:1,000), rabbit anti-acetyl-cMyc (Sigma ABE26; 1:1,000), rabbit anti-cMyc (CST 18583; 1:1,000), mouse anti-acetylated lysine (CST 9681; 1:1,000), anti-β-actin HRP-conjugate (CST 5125; 1:10,000), HRP-linked anti-mouse IgG (CST 7076; 1:2,500) and anti-rabbit IgG HRP-linked (CST 7074; 1:2,500). Blots were imaged with film and quantified by ImageJ.

Immunoprecipitation

BMDMs were lysed in Pierce IP lysis buffer (ThermoFisher) supplemented with a protease and phosphatase inhibitor cocktail (ThermoFisher). Lysates were homogenized through a 25G needle five times and incubated on a rotator for 15 min at 4 °C. Lysates were then centrifuged at 16,000*g* for 10 min at 4 °C, and the supernates were transferred to a fresh tube. Next, 10 µl of Pierce protein A/G magnetic beads crosslinked to equal amounts of either control rabbit IgG (CST 3900; 1:250) or anti-cMyc (CST 18583; 1:100) were added to the supernates and incubated overnight at 4 °C with rotation. The beads were washed five times by centrifugation with lysis buffer, and then protein was eluted with 50 µl of 0.1% RapiGest SF surfactant (Waters, catalogue no. 186001861) in 200 mM Tris pH 8.0. Laemmli sample buffer (4×) was added to the eluted protein, and the solution was then boiled and used for immunoblot analysis.

Immunofluorescence staining and microscopy

BMDMs that were transfected with scrambled or Ldha siRNA were seeded on eight-well chamber slides at 60,000 cells per well before incubation with PKH26-labelled ACs and chased for 3 h. The cells were fixed for 10 min at room temperature in 4% paraformaldehyde. Fixed cells were rinsed with PBS and then permeabilized with 0.25% Triton X-100 for 10 min at room temperature, blocked with 2% BSA in PBS for 1 h at room temperature, and incubated with Myc primary antibody (CST 18583; 1:100) in blocking solution at 4 °C overnight. The cells were then rinsed with PBS and incubated with chicken anti-rabbit AF647 secondary antibody (Invitrogen, catalogue no. A-21443) for 1 h at room temperature in the dark. Cells were rinsed again with PBS and then stained with Hoechst-33342 (CST 4082; 1:1,000) for 15 min at room temperature before mounting and imaging. For paraffin-embedded tissues, sections were deparaffinized with xylene, rehydrated with 100% ethanol and then 70% ethanol, and rinsed with PBS. Antigen retrieval was performed using 1x Citrate-Based Antigen Unmasking Solution (Vector) and pressure cooking for 10 min. TUNEL staining was conducted following antigen retrieval using the In Situ Cell Death Detection Kit (Sigma) according to the manufacturer's instructions. The tissues were blocked with 2% BSA in PBS for 1 h at room temperature and incubated overnight at 4 °C with primary antibody in blocking solution. The following primary antibodies were used: rabbit anti-cMyc (CST 18583; 1:100), rabbit anti-LDHA (ProteinTech, catalogue no. 19987-1-AP; 1:100), rabbit anti-Ki67 (ab16667; 1:200) and rat anti-Mac2 (Cedarlane, catalogue no. CL8942LE; 1:500). Tissues were rinsed with PBS and incubated for 2 h at room temperature with fluorescently labelled secondary antibody diluted in blocking solution. The following secondary antibodies were used: goat anti-rabbit AF488 (Invitrogen catalogue no. A11034; 1:200), and goat anti-rat AF647 (Invitrogen, catalogue no. A21247; 1:200). All imaging was performed using a Leica epifluorescence microscope (catalogue no. DMI6000B).

NAD^+ to NADH ratio assay

NAD^+ to NADH ratio was quantified using an NAD/NADH colorimetric assay kit (Abcam). Briefly, WT BMDMs, *Ldha*$^{fl/fl}$ BMDMs, or *Ldha*$^{fl/fl}$; *LysMCre*$^{+/-}$ BMDMs were seeded at 2,000,000 per well in six-well plates and incubated with unlabelled ACs, washed with PBS and chased for 1 h with or without 10 µM Compound C (Sigma) or 10 mM lactic acid (Sigma). The cells were collected with 400 µl of NADH/NAD extraction buffer from the kit, and the assay was conducted according to the manufacturer's instructions. SoftMax Pro Software v.5.4.l was used to analyse the data for this assay.

SIRT1 activity assay

SIRT1 activity was measured using a SIRT1 activity assay kit (Abcam) according to the manufacturer's instructions. Briefly, WT BMDMs were seeded at 4,000,000 per dish in 100 mm dishes and incubated with unlabelled ACs, washed with PBS and chased for 1 h with or without 50 µM FX11 (Sigma), 10 mM lactic acid (Sigma) or 10 µM Compound C (Sigma). Nuclear fractions were isolated and assessed for SIRT1 activity by measuring the fluorescence with an excitation wavelength of 350 nm and emission wavelength of 450 nm. SoftMax Pro Software v.5.4.l was used to analyse the data for this assay.

Efferocytosis assay

Macrophages were incubated with PKH26-labelled ACs for 45 min and then rinsed with PBS to remove unbound ACs and fixed with 4% PFA for 10 min at room temperature. After rinsing again with PBS, the macrophages were subjected to brightfield and fluorescence imaging using a Leica DMI6000B inverted epifluorescence microscope to identify macrophages that had taken up a fluorescent AC. AC uptake was quantified as the percentage of AC-positive macrophages out of the total number of macrophages per field of view.

RT–qPCR

RNA was isolated from macrophages using the PureLink RNA Mini kit (Life Technologies) according to the manufacturer's protocol. The RNA quality and concentration was measured using a NanoDrop spectrophotometer (ThermoFisher). Complementary DNA synthesis was generated from RNA using oligo(dT) and Superscript II (Applied Biosystems). RT–qPCR (reverse transcription with quantitative PCR) was conducted using the 7500 Real-Time PCR system (Applied Biosystems) and the Power SYBR Green PCR Master Mix (Applied Biosystems). The primers are listed in Supplementary Table 1. Expression of genes of interest were normalized to the expression of the housekeeping gene *Hprt*.

Statistical analyses

GraphPad Prism software (v.9.4.0 and v.9.4.1) was used for all statistical analyses. Data were tested for normality using the Shapiro–Wilk test. Data that passed the normality test were analysed using the two-tailed

Student's *t*-test for comparison of two groups or one- or two-way analysis of variance (ANOVA) with Bonferroni post hoc analysis for comparison of more than two groups. Data that were not normally distributed were analysed using the Mann–Whitney test. Data are shown as mean values ± s.e.m. and differences were considered statistically significant at $P < 0.05$. For normalization of data, all values were divided by the mean of the control group. No data were excluded. Data collection and analysis were not performed blind to the conditions of the experiments. The number of mice used for the dexamethasone-thymus assay was determined on the basis of power calculations, with an expected 15–25% coefficient of variation and an 80% chance of detecting a 33% difference in key parameters, including in situ efferocytosis and necrotic area. For the cell culture studies, no statistical methods were used to predetermine sample sizes, but our sample sizes are similar to those reported in previous publications[9,10]. For all experiments, *n* represents the number of independent replicates.

Reporting summary

Further information on research design is available in the Nature Portfolio Reporting Summary linked to this article.

Data availability

All data supporting the present study are available within the paper and supplementary information files. Source data are provided with this paper.

References

1. Morioka, S., Maueröder, C. & Ravichandran, K. S. Living on the edge: efferocytosis at the interface of homeostasis and pathology. *Immunity* **50**, 1149–1162 (2019).
2. Doran, A. C., Yurdagul, A. & Tabas, I. Efferocytosis in health and disease. *Nat. Rev. Immunol.* **20**, 254–267 (2020).
3. Arandjelovic, S. & Ravichandran, K. S. Phagocytosis of apoptotic cells in homeostasis. *Nat. Immunol.* **16**, 907–917 (2015).
4. Boada-Romero, E., Martinez, J., Heckmann, B. L. & Green, D. R. The clearance of dead cells by efferocytosis. *Nat. Rev. Mol. Cell Biol.* **21**, 398–414 (2020).
5. Dalli, J. & Serhan, C. N. Pro-resolving mediators in regulating and conferring macrophage function. *Front. Immunol.* **8**, 1400 (2017).
6. Colegio, O. R. et al. Functional polarization of tumour-associated macrophages by tumour-derived lactic acid. *Nature* **513**, 559–563 (2014).
7. Cai, H. et al. Moderate l-lactate administration suppresses adipose tissue macrophage M1 polarization to alleviate obesity-associated insulin resistance. *J. Biol. Chem.* **298**, 101768 (2022).
8. Morioka, S. et al. Efferocytosis induces a novel SLC program to promote glucose uptake and lactate release. *Nature* **563**, 714–718 (2018).
9. Schilperoort, M., Ngai, D., Katerelos, M., Power, D. A. & Tabas, I. PFKFB2-mediated glycolysis promotes lactate-driven continual efferocytosis by macrophages. *Nat. Metab.* **5**, 431–444 (2023).
10. Gerlach, B. D. et al. Efferocytosis induces macrophage proliferation to help resolve tissue injury. *Cell Metab.* **33**, 2445–2463.e2448 (2021).
11. Yurdagul, A. Jr et al. Macrophage metabolism of apoptotic cell-derived arginine promotes continual efferocytosis and resolution of injury. *Cell Metab.* **31**, 518–533.e10 (2020).
12. Zhang, S. et al. Efferocytosis fuels requirements of fatty acid oxidation and the electron transport chain to polarize macrophages for tissue repair. *Cell Metab.* **29**, 443–456.e445 (2019).
13. Farrell, A. S. & Sears, R. C. MYC degradation. *Cold Spring Harb. Perspect. Med.* **4**, a014365 (2014).
14. Marshall, G. M. et al. SIRT1 promotes N-Myc oncogenesis through a positive feedback loop involving the effects of MKP3 and ERK on N-Myc protein stability. *PLoS Genet.* **7**, e1002135 (2011).
15. Menssen, A. et al. The c-MYC oncoprotein, the NAMPT enzyme, the SIRT1-inhibitor DBC1, and the SIRT1 deacetylase form a positive feedback loop. *Proc. Natl Acad. Sci. USA* **109**, E187–E196 (2012).
16. Li, L. et al. SIRT1 activation by a c-MYC oncogenic network promotes the maintenance and drug resistance of human FLT3-ITD acute myeloid leukemia stem cells. *Cell Stem Cell* **15**, 431–446 (2014).
17. Nebbioso, A. et al. c-Myc modulation and acetylation is a key HDAC inhibitor target in cancer. *Clin. Cancer Res.* **23**, 2542–2555 (2017).
18. Mao, B. et al. Sirt1 deacetylates c-Myc and promotes c-Myc/Max association. *Int. J. Biochem. Cell Biol.* **43**, 1573–1581 (2011).
19. Zhang, Y. & Dong, F. Gfi1 upregulates c-Myc expression and promotes c-Myc-driven cell proliferation. *Sci. Rep.* **10**, 17115 (2020).
20. Yang, L. et al. Lactate promotes synthetic phenotype in vascular smooth muscle cells. *Circ. Res.* **121**, 1251–1262 (2017).
21. Watson, M. J. et al. Metabolic support of tumour-infiltrating regulatory T cells by lactic acid. *Nature* **591**, 645–651 (2021).
22. Le, A. et al. Inhibition of lactate dehydrogenase A induces oxidative stress and inhibits tumor progression. *Proc. Natl Acad. Sci. USA* **107**, 2037–2042 (2010).
23. McCubbrey, A. L. et al. MicroRNA-34a negatively regulates efferocytosis by tissue macrophages in part via SIRT1. *J Immunol.* **196**, 1366–1375 (2016).
24. El Hayek, L. et al. Lactate mediates the effects of exercise on learning and memory through SIRT1-dependent activation of hippocampal brain-derived neurotrophic factor (BDNF). *J. Neurosci.* **39**, 2369–2382 (2019).
25. Gertz, M. et al. Ex-527 inhibits Sirtuins by exploiting their unique NAD^+-dependent deacetylation mechanism. *Proc. Natl Acad. Sci. USA* **110**, E2772–E2781 (2013).
26. López-Villegas, D., Lenkinski, R. E., Wehrli, S. L., Ho, W. Z. & Douglas, S. D. Lactate production by human monocytes/macrophages determined by proton MR spectroscopy. *Magn. Reson. Med.* **34**, 32–38 (1995).
27. Roussel, M. F. Signal transduction by the macrophage-colony-stimulating factor receptor (CSF-1R). *J. Cell Sci. Suppl.* **18**, 105–108 (1994).
28. Stanley, E. R. & Chitu, V. CSF-1 receptor signaling in myeloid cells. *Cold Spring Harb. Perspect. Biol.* **6**, a021857 (2014).
29. Cantó, C. et al. AMPK regulates energy expenditure by modulating NAD^+ metabolism and SIRT1 activity. *Nature* **458**, 1056–1060 (2009).
30. Costford, S. R. et al. Skeletal muscle NAMPT is induced by exercise in humans. *Am. J. Physiol. Endocrinol. Metab.* **298**, E117–E126 (2010).
31. Cerda-Kohler, H. et al. Lactate administration activates the ERK1/2, mTORC1, and AMPK pathways differentially according to skeletal muscle type in mouse. *Physiol. Rep.* **6**, e13800 (2018).
32. Jiang, S. et al. Mitochondria and AMP-activated protein kinase-dependent mechanism of efferocytosis. *J. Biol. Chem.* **288**, 26013–26026 (2013).
33. Garcia, D. & Shaw, R. J. AMPK: mechanisms of cellular energy sensing and restoration of metabolic balance. *Mol. Cell* **66**, 789–800 (2017).
34. Foster, J. R. et al. N-palmitoylglycine and other N-acylamides activate the lipid receptor G2A/GPR132. *Pharmacol. Res. Perspect.* **7**, e00542 (2019).

35. Nii, T. et al. Imipridone ONC212 activates orphan G protein-coupled receptor GPR132 and integrated stress response in acute myeloid leukemia. *Leukemia* **33**, 2805–2816 (2019).
36. Ampomah, P. B. et al. Macrophages use apoptotic cell-derived methionine and DNMT3A during efferocytosis to promote tissue resolution. *Nat. Metab.* **4**, 444–457 (2022).
37. Kasikara, C. et al. Deficiency of macrophage PHACTR1 impairs efferocytosis and promotes atherosclerotic plaque necrosis. *J. Clin. Invest.* **131**, e145275 (2021).
38. Park, D. et al. Continued clearance of apoptotic cells critically depends on the phagocyte Ucp2 protein. *Nature* **477**, 220–224 (2011).
39. Yurdagul, A., Doran, A. C., Cai, B., Fredman, G. & Tabas, I. A. Mechanisms and consequences of defective efferocytosis in atherosclerosis. *Front. Cardiovasc. Med.* **4**, 86 (2017).
40. Vadevoo, S. M. P. et al. The macrophage odorant receptor Olfr78 mediates the lactate-induced M2 phenotype of tumor-associated macrophages. *Proc. Natl Acad. Sci. USA* **118**, e2102434118 (2021).
41. Sag, D., Carling, D., Stout, R. D. & Suttles, J. Adenosine 5′-monophosphate-activated protein kinase promotes macrophage polarization to an anti-inflammatory functional phenotype. *J. Immunol.* **181**, 8633–8641 (2008).
42. Jha, M. K. et al. Macrophage monocarboxylate transporter 1 promotes peripheral nerve regeneration after injury in mice. *J. Clin. Invest.* **131**, e141964 (2021).
43. Wang, Y. et al. Mitochondrial fission promotes the continued clearance of apoptotic cells by macrophages. *Cell* **171**, 331–345. e322 (2017).
44. Li, X. et al. Lactate metabolism in human health and disease. *Signal Transduct. Target. Ther.* **7**, 305 (2022).
45. Brooks, G. A. Lactate as a fulcrum of metabolism. *Redox Biol.* **35**, 101454 (2020).
46. Sharma, M. et al. Regulatory T cells license macrophage pro-resolving functions during atherosclerosis regression. *Circ. Res.* **127**, 335–353 (2020).
47. Newby, A. C. & Zaltsman, A. B. Fibrous cap formation or destruction–the critical importance of vascular smooth muscle cell proliferation, migration and matrix formation. *Cardiovasc. Res.* **41**, 345–360 (1999).
48. Haas, R. et al. Lactate regulates metabolic and pro-inflammatory circuits in control of T cell migration and effector functions. *PLoS Biol.* **13**, e1002202 (2015).
49. Skuljec, J. et al. Absence of regulatory T cells causes phenotypic and functional switch in murine peritoneal macrophages. *Front. Immunol.* **9**, 2458 (2018).
50. Proto, J. D. et al. Regulatory T cells promote macrophage efferocytosis during inflammation resolution. *Immunity* **49**, 666–677.e666 (2018).
51. Miao, P., Sheng, S., Sun, X., Liu, J. & Huang, G. Lactate dehydrogenase A in cancer: a promising target for diagnosis and therapy. *IUBMB Life* **65**, 904–910 (2013).
52. Sinha, S. K. et al. Local M-CSF (macrophage colony-stimulating factor) expression regulates macrophage proliferation and apoptosis in atherosclerosis. *Arterioscler. Thromb. Vasc. Biol.* **41**, 220–233 (2021).
53. Shantha, G. P. et al. Association of blood lactate with carotid atherosclerosis: the Atherosclerosis Risk in Communities (ARIC) Carotid MRI Study. *Atherosclerosis* **228**, 249–255 (2013).
54. Garcia-Alvarez, M., Marik, P. & Bellomo, R. Sepsis-associated hyperlactatemia. *Crit. Care* **18**, 503 (2014).
55. Tabas, I. Consequences and therapeutic implications of macrophage apoptosis in atherosclerosis: the importance of lesion stage and phagocytic efficiency. *Arterioscler. Thromb. Vasc. Biol.* **25**, 2255–2264 (2005).
56. Cui, X. et al. The G2A receptor deficiency aggravates atherosclerosis in rats by regulating macrophages and lipid metabolism. *Front. Physiol.* **12**, 659211 (2021).
57. Koyama, T. Lactated Ringer's solution for preventing myocardial reperfusion injury. *Int. J. Cardiol. Heart Vasc.* **15**, 1–8 (2017).
58. Gleeson, M. et al. The anti-inflammatory effects of exercise: mechanisms and implications for the prevention and treatment of disease. *Nat. Rev. Immunol.* **11**, 607–615 (2011).
59. Casteels, K. M. et al. Sex difference in resistance to dexamethasone-induced apoptosis in NOD mice: treatment with 1,25(OH)2D3 restores defect. *Diabetes* **47**, 1033–1037 (1998).

Acknowledgements

This work was supported by an American Heart Association Postdoctoral Fellowship (grant no. 900337 to M.S.); the Niels Stensen Fellowship (to M.S.) and NIH/NHLBI grant nos. R35-HL145228 and P01-HL087123 (to I.T.). We thank L. Becker (University of Chicago) for providing *Ldha*$^{fl/fl}$ and *Ldha*$^{fl/fl}$*; LysMCre*$^{+/-}$ mouse femurs for BMDM differentiation to use in our in vitro studies. We thank X. Wang (Columbia University) for assisting with intravenous injections for BMT. We acknowledge C. Lu of the Columbia Center for Translational Immunology Core Facility for assisting in the immunofluorescent imaging experiments that were conducted in the Columbia Center for Translational Immunology Core Facility, funded by NIH grant nos. P30CA013696, S10RR027050 and S10OD020056.

Author contributions

D.N. and I.T. conceived the project. D.N., M.S. and I.T. provided intellectual input to the development of the project. D.N. performed the in vitro experiments. D.N. and M.S. performed the in vivo dexamethasone-thymus experiment.

Competing interests

The authors declare no competing interests.

Additional information

Extended data is available for this paper at https://doi.org/10.1038/s42255-023-00921-9.

Supplementary information The online version contains supplementary material available at https://doi.org/10.1038/s42255-023-00921-9.

Correspondence and requests for materials should be addressed to David Ngai or Ira Tabas.

Peer review information *Nature Metabolism* thanks Roel De Maeyer, Nicholas Leeper and Feilong Wang for their contribution to the peer review of this work. Primary Handling Editor: Alfredo Giménez-Cassina, in collaboration with the *Nature Metabolism* team.

https://doi.org/10.1038/s42255-023-00921-9

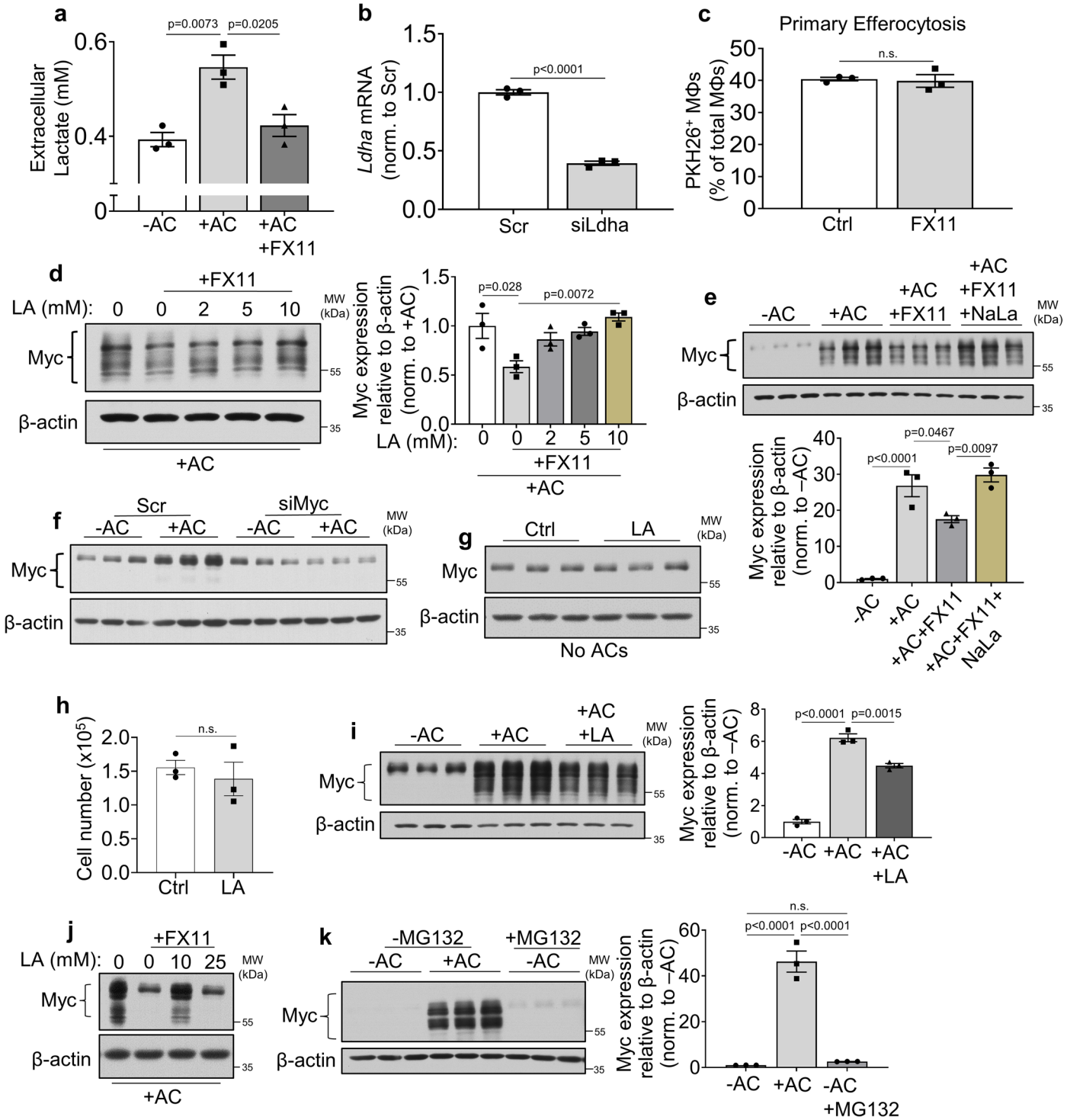

Extended Data Fig. 1 | Related to Figs. 1 and 2: Controls for BMDM experiments. a, BMDMs were incubated with or without ACs for 45 minutes before washing and chasing for 1 hour in low-serum DMEM ± 50 μM FX11. The media were assayed for lactate concentration (n = 3). **b**, BMDMs were transfected with scrambled (Scr) or Ldha siRNA for 72 hours and then assayed for *Ldha* mRNA by RT-qPCR (n = 3). **c)** BMDMs pre-treated with 50 μM FX11 for 1 hour were incubated for 45 minutes with PKH26-labelled ACs and quantified for % $PKH26^+$ macrophages (n = 3). **d**, BMDMs were incubated with ACs for 45 minutes, chased for 3 hours ± 50 μM FX11 and ± 2/5/10 mM LA, and immunoblotted for Myc (n = 3). **e**, BMDMs were incubated with or without ACs for 45 minutes, chased for 3 hours ± 50 μM FX11 and ± 10 mM sodium lactate (NaLa), and immunoblotted for Myc (n = 3). **f**, BMDMs transfected with 50 nM scrambled or Myc siRNA for 72 hours were incubated with or without ACs for 45 minutes, chased for 3 hours, and immunoblotted for Myc (n = 3). **g**, BMDMs were treated ± 10 mM LA for 3 hours and immunoblotted for Myc (n = 3). **h**, BMDMs were treated for 24 hours ± 10 mM LA before performing a cell count (n = 3). **i**, BMDMs were incubated with or without ACs for 45 minutes, chased for 3 hours ± 10 mM LA, and immunoblotted for Myc (n = 3). **j**, BMDMs were incubated with ACs for 45 minutes, chased for 3 hours ± 50 μM FX11 and ± 10 or 25 mM LA, and immunoblotted for Myc. Similar results were obtained in a repeat experiment. **k**, BMDMs were incubated with or without ACs for 45 minutes, chased for 3 hours ± 10 μM MG132, and immunoblotted for Myc (n = 3). Bars represent means ± s.e.m. Statistics were performed by two-tailed student's t-test in panels **b-c**, **h**, or one-way ANOVA in panels **a**, **d**, **e**, **i**, and **k**. n.s. = non-significant ($P > 0.05$).

https://doi.org/10.1038/s42255-023-00921-9

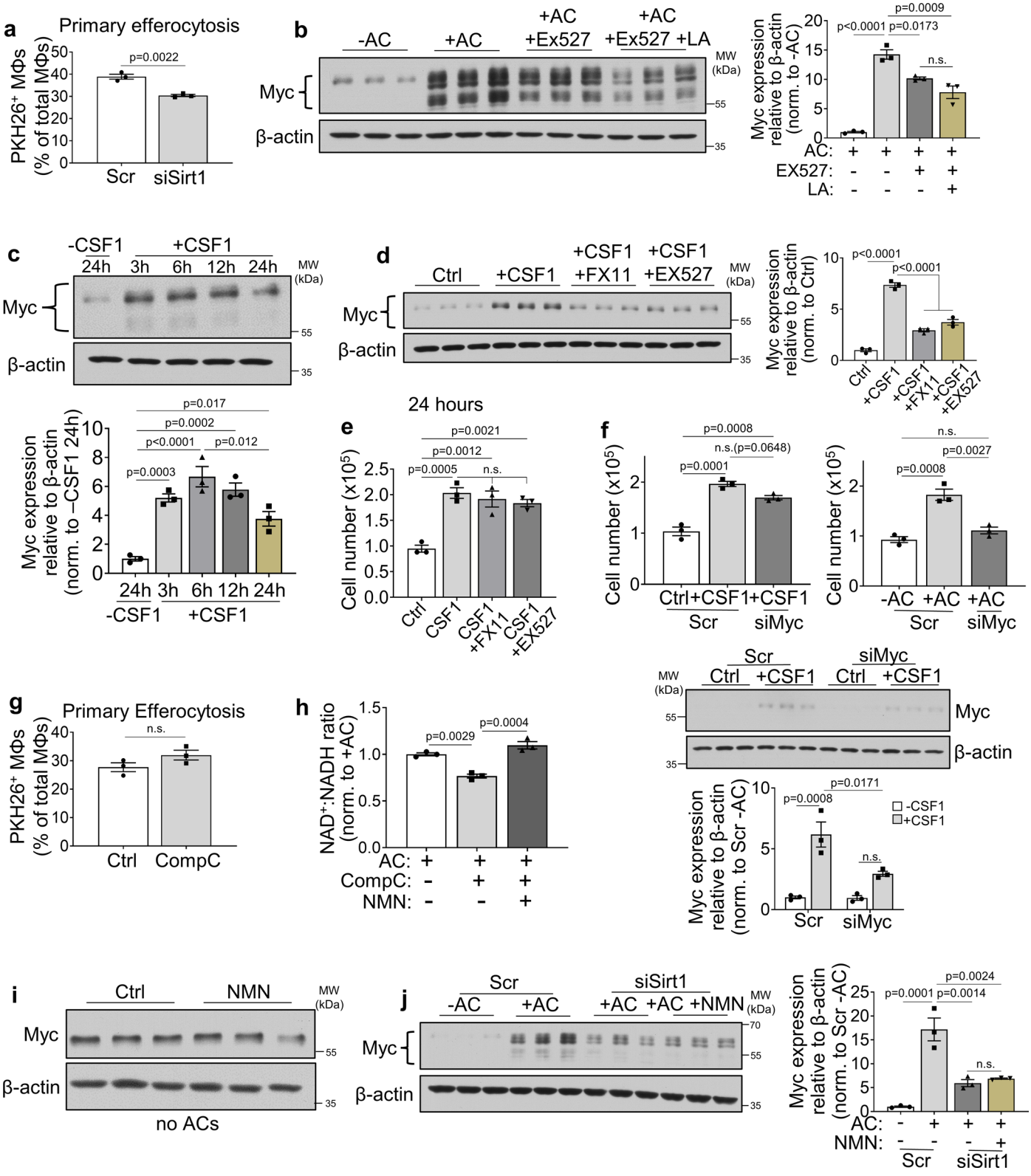

Extended Data Fig. 2 | See next page for caption.

https://doi.org/10.1038/s42255-023-00921-9

Extended Data Fig. 2 | Related to Figs. 3 and 4: Controls for BMDM experiments. a, BMDMs were transfected with 50 nM scrambled or Sirt1 siRNA for 72 hours, incubated with PKH26-labelled ACs for 45 minutes, and quantified for the percent $PKH26^+$ macrophages (n = 3). **b**, BMDMs were incubated with or without ACs for 45 minutes, chased for 3 hours ± 10 μM EX527 and ± 10 mM LA, and immunoblotted for Myc (n = 3). **c**, BMDMs were treated with 50 ng/mL CSF-1 for 3, 6, 12, or 24 hours and immunoblotted for Myc. The image presented is one representative replicate (n = 3). **d**, BMDMs were treated with or without 50 ng/mL CSF-1 + 50 μM FX11 or 10 μM EX527, and immunoblotted for Myc (n = 3). **e**, BMDMs were treated for 24 hours with 50 ng/mL CSF-1 + 50 μM FX11 or 10 μM EX527, and quantified for cell number (n = 3). **f**, BMDMs were transfected with 50 nM scrambled or Myc siRNA for 72 hours, incubated ± ACs for 45 minutes or with CSF-1, and then assayed 24 hours later for cell number and Myc protein for CSF1-treated cells (n = 3). **g**, BMDMs pre-treated for 1 hour with 10 μM CompC were incubated with PKH26-labelled ACs and quantified for the percent $PKH26^+$ (n = 3). **h**, BMDMs were chased for 1 hour + 10 μM CompC with or without 500 μM NMN and then assayed for NAD^+ to NADH ratio (n = 3). **i**, BMDMs were treated ± 500 μM NMN for 3 hours and then immunoblotted for Myc (n = 3). **j**, BMDMs transfected with scrambled or Sirt1 siRNA were chased for 3 hours ± 500 μM NMN and then immunoblotted for Myc (n = 3). Bars represent means ± s.e.m. Statistics were performed by two-tailed student's t-test in panels **a** and **g**, or one-way ANOVA in panels **b**-**f**, **h**, and **j**. n.s. = non-significant ($P > 0.05$).

https://doi.org/10.1038/s42255-023-00921-9

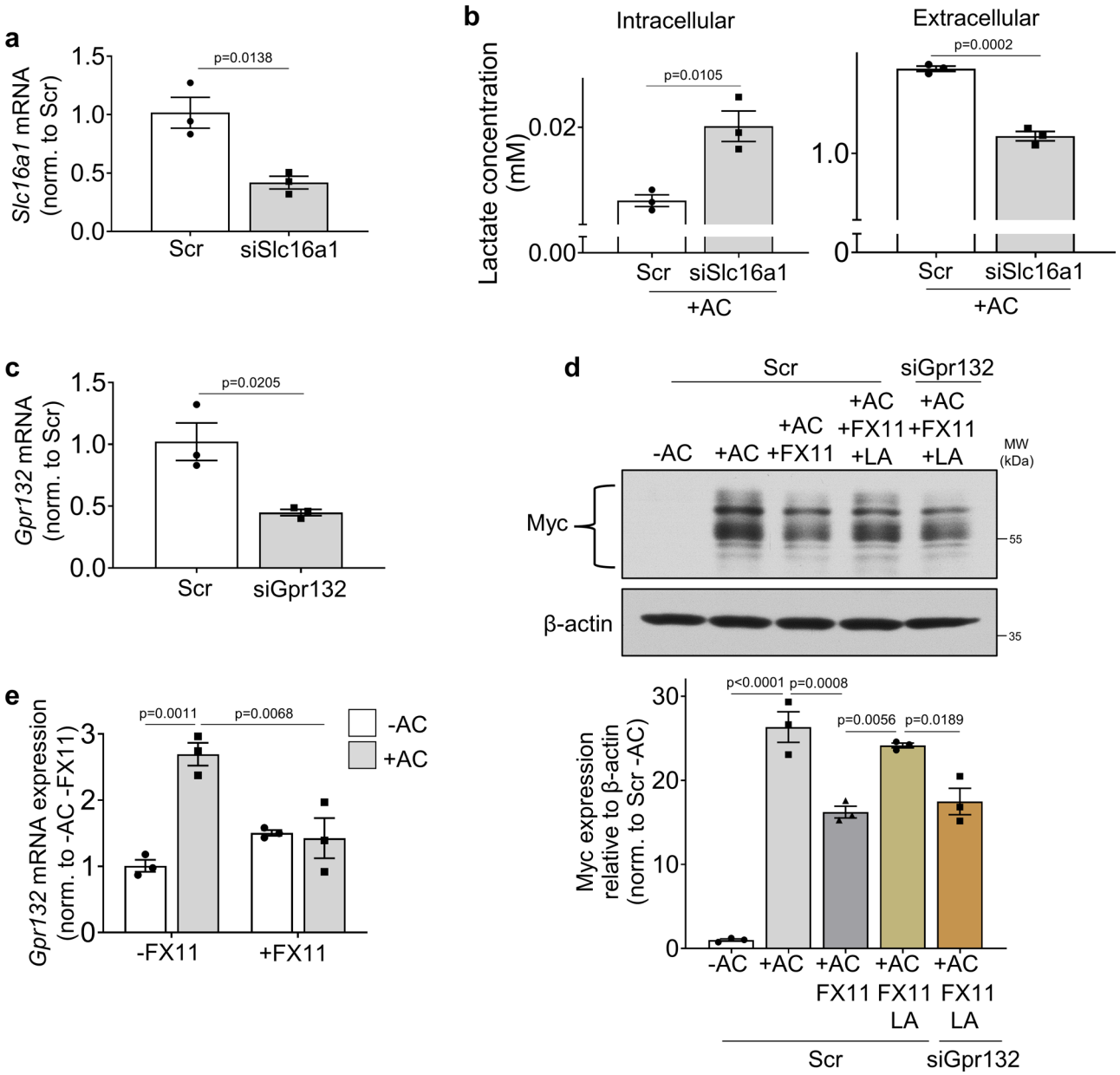

Extended Data Fig. 3 | Related to Fig. 5: Controls for BMDM experiments. **a**, BMDMs were transfected with 50 nM scrambled or Slc16a1 siRNA for 72 hours and then assayed for *Slc16a1* mRNA by RT-qPCR (n = 3). **b**, BMDMs transfected with 50 nM scrambled or Slc16a1 siRNA for 72 hours were incubated with ACs for 45 minutes, chased for 3 hours in 1% FBS DMEM before collecting supernatants and cell lysates to measure intracellular and extracellular lactate concentrations (n = 3). **c**, BMDMs were transfected with 50 nM scrambled or Gpr132 siRNA for 72 hours and then assayed for *Gpr132* mRNA by RT-qPCR (n = 3). **d**, BMDMs transfected with 50 nM scrambled or Gpr132 siRNA for 72 hours were incubated with or without ACs for 45 minutes, chased for 3 hours ± 50 μM FX11 and ± 10 mM LA, and immunoblotted for Myc. The displayed immunoblot is a representative replicate (n = 3). **e**, BMDMs were incubated with or without ACs for 45 minutes, chased for 3 hours ± 50 μM FX11, and assayed for *Gpr132* mRNA (n = 3). Bars represent means ± s.e.m. Statistics were performed by two-tailed student's t-test in panels **a**-**c**, one-way ANOVA in panel **d**, or two-way ANOVA in panel **e**. n.s. = non-significant ($P > 0.05$).

https://doi.org/10.1038/s42255-023-00921-9

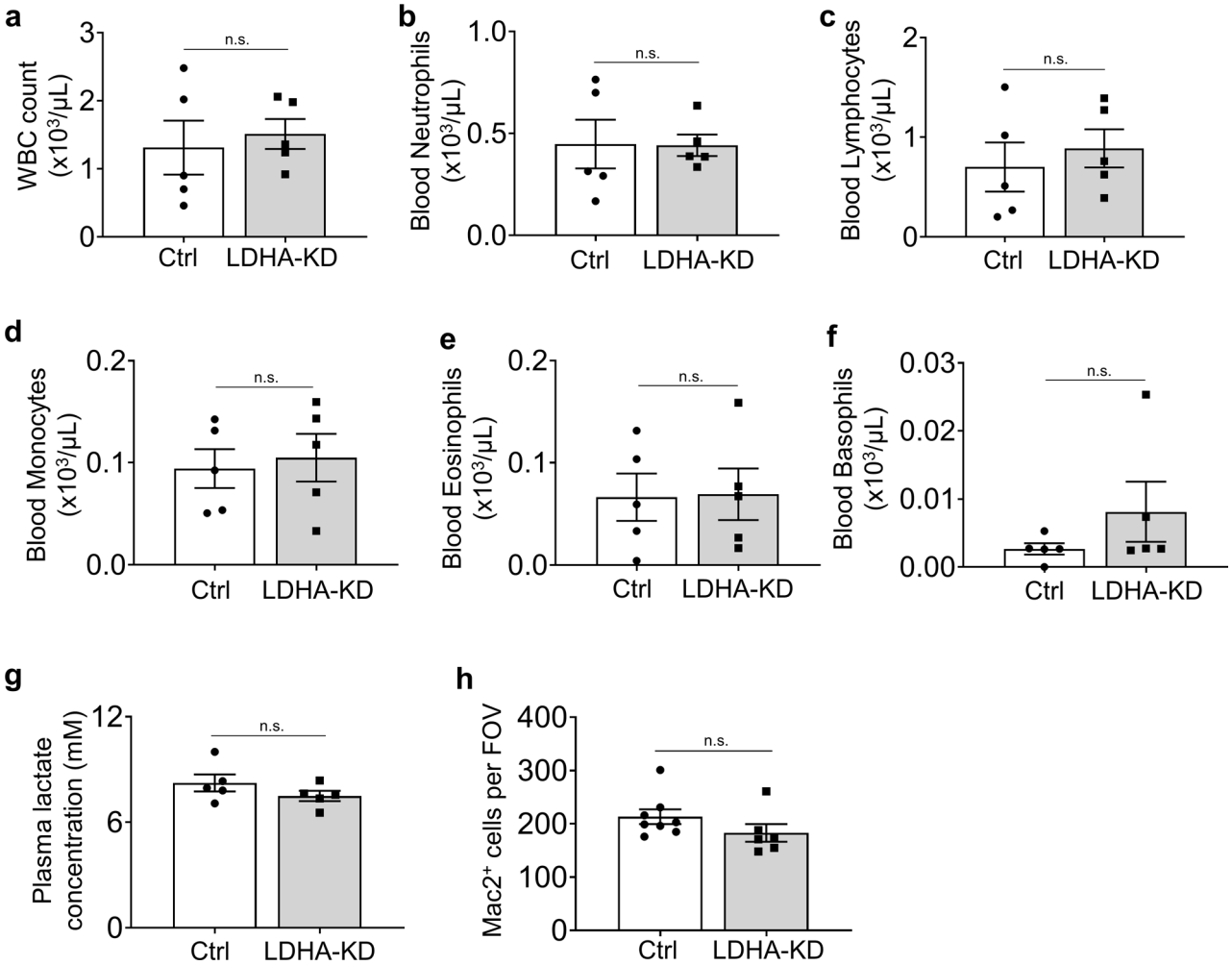

Extended Data Fig. 4 | Related to Fig. 6: Controls and blood counts for the dexamethasone-thymus experiment. a-f, Counts of blood WBCs, neutrophils, lymphocytes, monocytes, eosinophils, and basophils (n = 5). **g**, Plasma was measured for lactate concentration (n = 5). **h**, Mac2$^+$ cells in immunostained thymus sections were counted per field of view (FOV) using images taken with a 20x objective (n = 8,6). Bars represent means ± s.e.m. Statistics were performed by two-tailed student's t-test in panels **a**-**e** and **g**-**h**, and Mann–Whitney test for panel **f**. n.s. = non-significant ($P > 0.05$).

nature portfolio

Corresponding author(s): Dr. David Ngai and Dr. Ira Tabas

Last updated by author(s): September 1, 2023

Reporting Summary

Nature Portfolio wishes to improve the reproducibility of the work that we publish. This form provides structure for consistency and transparency in reporting. For further information on Nature Portfolio policies, see our Editorial Policies and the Editorial Policy Checklist.

Statistics

For all statistical analyses, confirm that the following items are present in the figure legend, table legend, main text, or Methods section.

n/a	Confirmed	
☐	☒	The exact sample size (*n*) for each experimental group/condition, given as a discrete number and unit of measurement
☐	☒	A statement on whether measurements were taken from distinct samples or whether the same sample was measured repeatedly
☐	☒	The statistical test(s) used AND whether they are one- or two-sided *Only common tests should be described solely by name; describe more complex techniques in the Methods section.*
☒	☐	A description of all covariates tested
☐	☒	A description of any assumptions or corrections, such as tests of normality and adjustment for multiple comparisons
☐	☒	A full description of the statistical parameters including central tendency (e.g. means) or other basic estimates (e.g. regression coefficient) AND variation (e.g. standard deviation) or associated estimates of uncertainty (e.g. confidence intervals)
☐	☒	For null hypothesis testing, the test statistic (e.g. *F*, *t*, *r*) with confidence intervals, effect sizes, degrees of freedom and *P* value noted *Give P values as exact values whenever suitable.*
☒	☐	For Bayesian analysis, information on the choice of priors and Markov chain Monte Carlo settings
☒	☐	For hierarchical and complex designs, identification of the appropriate level for tests and full reporting of outcomes
☒	☐	Estimates of effect sizes (e.g. Cohen's *d*, Pearson's *r*), indicating how they were calculated

Our web collection on statistics for biologists contains articles on many of the points above.

Software and code

Policy information about availability of computer code

Data collection	Applied Biosystems 7500 software v. 2.3 was used to collect qRT-PCR data. Leica LAS AF v. 1.9.0 was used to collect epifluorescent microscope images. SoftMax Pro Software v. 5.4.1 was used to collect data for the NAD+:NADH ratio assay and SIRTl activity assay.
Data analysis	ImageJ 2 2.9.0 was used for analysis of immunofluorescent images and Western blot densitometry. Statistical analysis was performed using GraphPad Prism Versions 9.4.0 and 9.4.1.

For manuscripts utilizing custom algorithms or software that are central to the research but not yet described in published literature, software must be made available to editors and reviewers. We strongly encourage code deposition in a community repository (e.g. GitHub). See the Nature Portfolio guidelines for submitting code & software for further information.

Data

Policy information about availability of data

All manuscripts must include a data availability statement. This statement should provide the following information, where applicable:

- Accession codes, unique identifiers, or web links for publicly available datasets
- A description of any restrictions on data availability
- For clinical datasets or third party data, please ensure that the statement adheres to our policy

All data supporting this study are available within the manuscript and supplementary information files. Source data are provided within this paper.

Human research participants

Policy information about studies involving human research participants and Sex and Gender in Research.

Reporting on sex and gender	Human monocyte-derived macrophages were obtained from the blood collected from anonymous adult volunteers (unknown sex and gender).
Population characteristics	Unknown (donors are completely unidentifiable by us).
Recruitment	Blood was collected by the New York Blood Center.
Ethics oversight	Blood was collected with informed consent, and the University Institutional Review Board and Health Insurance Portability and Accountability Act guidelines were followed. This is not considered "human research" as it is exempted based on the Protection of Human Rights Title 45 CFR 46.104, section 4 (ii).

Note that full information on the approval of the study protocol must also be provided in the manuscript.

Field-specific reporting

Please select the one below that is the best fit for your research. If you are not sure, read the appropriate sections before making your selection.

☒ Life sciences ☐ Behavioural & social sciences ☐ Ecological, evolutionary & environmental sciences

For a reference copy of the document with all sections, see nature.com/documents/nr-reporting-summary-flat.pdf

Life sciences study design

All studies must disclose on these points even when the disclosure is negative.

Sample size	Previous studies and pilot data from the lab formed the basis of power calculations for the experiments in this manuscript. For the dexamethasone-thymus experiment, calculations indicated that 6-8 mice per group would allow us to test the main hypotheses based on an expected 15-25% coefficient of variation and an 80% chance of detecting 33% differences in the key specified endpoints (p = 0.05). 2 mice from the LDHA-KD group were sacrificed 4 weeks after bone marrow transplantation and prior to the dexamethasone-thymus experiment to check for KD efficiency in blood cells and bone marrow cells.
Data exclusions	No data was excluded.
Replication	All experiments were reproducible as assessed by multiple wells of cells, tissues, or mice. For in vitro assays, experiments involved 3 or more biological replicates, and key experiments were repeated multiple times and proved reproducible. For the in vivo study, 6-8 mice were used per group. These numbers produced robust data and sufficient power for statistical analysis.
Randomization	Mice of the same age and similar weight were randomly assigned to experimental and control groups. Random vs. non-random assignment is not relevant to in vitro experiments.
Blinding	The main investigator was not blinded for the in vitro and in vivo studies. The main investigator was not blinded for the in vitro and in vivo studies for practical reasons, e.g., to apply different treatments such as PBS versus dexamethasone injection in mice.

Reporting for specific materials, systems and methods

We require information from authors about some types of materials, experimental systems and methods used in many studies. Here, indicate whether each material, system or method listed is relevant to your study. If you are not sure if a list item applies to your research, read the appropriate section before selecting a response.

Materials & experimental systems

n/a	Involved in the study
☐	☒ Antibodies
☐	☒ Eukaryotic cell lines
☒	☐ Palaeontology and archaeology
☐	☒ Animals and other organisms
☒	☐ Clinical data
☒	☐ Dual use research of concern

Methods

n/a	Involved in the study
☒	☐ ChIP-seq
☒	☐ Flow cytometry
☒	☐ MRI-based neuroimaging

Antibodies

Antibodies used

The host species, catalogue number, and vendors of all antibodies that were used in this paper have been provided in the Methods section and also provided below. The corresponding application for each dilution listed below are described as follows: WB (Western blot), IP (Immunoprecipitation), IF/ICC (Immunofluorescence/immunocytochemistry)

Rabbit anti-SIRT1 mAb (mouse) - Cell Signaling Technology #9475 - 1:1000 WB (Clone: D1D7)
Rabbit anti-LDHA pAb (mouse) - ProteinTech #19987-1-AP - 1:100 IF/ICC, 1:1000 WB
Rabbit anti-pAMPK mAB (mouse) - Cell Signaling Technology #2535 - 1:1000 WB (Clone: 40H9)
Rabbit anti-AMPK mAb (mouse) - Cell Signaling Technology #5831 - 1:1000 WB (Clone: D5A2)
Rabbit anti-pCREB mAb (mouse) - Cell Signaling Technology #9198 - 1:1000 WB (Clone: 87G3)
Rabbit anti-CREB mAb (mouse) - Cell Signaling Technology #4820 - 1:1000 WB (Clone: D76D11)
Rabbit anti-acetyl-Myc (mouse) - Sigma ABE26 - 1:1000 WB
Mouse anti-acetylated lysine (mouse) - Cell Signaling Technology #9681 - 1:1000 WB (Clone: Ac-K-103)
Rabbit anti-cMyc (mouse) - Cell Signaling Technology #18583 - 1:100 IF/ICC, 1:100 IP, 1:1000 WB (Clone: E5Q6W)
Rabbit anti-β-actin mAb HRP-conjugate - Cell Signaling Technology #5125 - 1:10,000 WB (Clone: 13E5)
Goat anti-rabbit HRP-linked secondary antibody - Cell Signaling Technology #7074 - 1:2500 WB
Horse anti-mouse HRP-linked secondary antibody - Cell Signaling Technology #7076 - 1:2500 WB
Rabbit anti-Ki67 mAb (mouse) - Abcam ab16667 - 1:200 IF/ICC (Clone: SP6)
Rat anti-Mac2 mAb (mouse) - Cedarlane CL8942LE - 1:500 IF/ICC (Clone: M3/38)
Goat anti-rabbit AlexaFluor488 secondary antibody - Invitrogen A11034 - 1:200 IF/ICC
Chicken anti-rabbit AlexaFluor647 secondary antibody - Invitrogen A21443 - 1:200 IF/ICC
Goat anti-rat AlexaFluor647 secondary antibody - Invitrogen A21247 - 1:200 IF/ICC
Rabbit mAb IgG XP isotype control - Cell Signaling Technology #3900 - 1:250 IP (Clone: DA1E)

Validation

All the antibodies are commercially available and have been validated by the manufacturer, other researchers, and/or by other members of the lab in published data. The following information is provided by the manufacturer with the tested applications described as follows: WB (Western blot), IP (immunoprecipitation), IF (immunofluorescence), ICC (immunocytochemistry), IHC (immunohistochemistry), FC (flow cytometry), ChIP (chromatin immunoprecipitation), C&R (CUT&RUN)

Cell SIgnaling Technology #9475 - Validated for WB, reacts with human, mouse, rat, monkey
ProteinTech #19987-1-AP - Validated for WB, IP, IHC, IF, and FC, reacts with human, mouse, rat
Cell Signaling Technology #2535 - Validated for WB, IP, and IHC, reacts with human, mouse, rat, hamster, monkey, drosophila, s. cerevisiae
Cell Signaling Technology #5831 - Validated for WB and IP, reacts with human, mouse, rat, monkey, bovine
Cell Signaling Technology #9198 - Validated for WB, IHC, IF, FC, ChIP, and C&R, reacts with human, mouse, rat
Cell Signaling Technology #4820 - Validated for WB, IP, IF, FC, and ChIP, reacts with human, mouse, rat, hamster, monkey, drosophila
Sigma ABE26 - Validated for WB, reacts with human and mouse
Cell Signaling Technology #9681 - Validated for WB, reacts with all species
Cell Signaling Technology #18583 - Validated for WB, IP, IF, FC, and ChIP, reacts with human, mouse, rat
Cell Signaling Technology #5125 - Validated for WB, reacts with human, mouse, rat, monkey, bovine, pig
Abcam ab16667 - Validated for WB, IHC, FC, IF, and ICC, reacts with human, mouse, rat
Cedarlane CL8942LE - Validated for WB, IF, FC, reacts with human, mouse

Eukaryotic cell lines

Policy information about cell lines and Sex and Gender in Research

Cell line source(s)

Human Jurkat T lymphocytes (ATCC TIB-152) and L-929 mouse fibroblasts (ATCC CCL-1).

Authentication

None of the cell lines used were authenticated.

Mycoplasma contamination

Cells were not tested for mycoplasma contamination.

Commonly misidentified lines
(See ICLAC register)

No commonly misidentified cell lines were used in this study.

Animals and other research organisms

Policy information about studies involving animals; ARRIVE guidelines recommended for reporting animal research, and Sex and Gender in Research

Laboratory animals

8-10 week old male C57BL/6J wild-type mice (JAX 000664) were used as the recipients of the bone marrow transplant performed prior to the dexamethasone-thymus experiment. Donor bone marrow cells were obtained from 8-10 week old male Ldha floxed mice on the C57BL/6J background (JAX 030112) treated with or without TAT-Cre ex vivo. The mice were group-housed in standard cages at 22°C with 40-60% humidity and under a 12:12 hr light/dark cycle with ad libitum access to water and food. Dr. Lev Becker provided us with femurs from 6-week old male Ldha floxed LysMCre het mice on the C57BL/6J background, or femurs from 6-week old male control Ldha floxed mice on the C57BL/6J background. Ldha floxed LysMCre het mice were generated by breeding Ldha floxed mice on the C57BL/6J background (JAX 030112) with LysMCre mice on the C57BL/6J background (JAX 004781).

Wild animals

No wild animals were used in this study.

Reporting on sex	Only male mice from Jackson Laboratory were used for experiments in this manuscript.
Field-collected samples	This study did not involve field-collected samples.
Ethics oversight	Animal protocols used for experiments were approved by Columbia University's Institutional Animal Care and Use Committee (protocol number AABL0571).

Note that full information on the approval of the study protocol must also be provided in the manuscript.